IEEE Access
Multidisciplinary ⋮ Rapid Review ⋮ Open Access Journal

Received December 7, 2020, accepted December 17, 2020, date of publication December 22, 2020,
date of current version January 4, 2021.

Digital Object Identifier 10.1109/ACCESS.2020.3046536

A Forensic-Based Investigation Algorithm for Parameter Extraction of Solar Cell Models

ABDULLAH M. SHAHEEN[1], AHMED RABIE GINIDI[1], RAGAB A. EL-SEHIEMY[2], (Senior Member, IEEE), AND SHERIF S. M. GHONEIM[3], (Senior Member, IEEE)

[1]Department of Electrical Engineering, Faculty of Engineering, Suez University, Suez 43518, Egypt
[2]Department of Electrical Engineering, Faculty of Engineering, Kafrelsheikh University, Kafrelsheikh 33516, Egypt
[3]Department of Electrical Engineering, College of Engineering, Taif University, Taif 21944, Saudi Arabia

Corresponding author: Ragab A. El-Sehiemy (elsehiemy@eng.kfs.edu.eg)

This work was supported by the Taif University, Taif, Saudi Arabia, through the Taif University Researchers Supporting Project, under Grant TURSP-2020/34.

ABSTRACT The accurate parameter extraction of photovoltaic (PV) module is pivotal for determining and optimizing the energy output of PV systems into electric power networks. Consequently, a Photovoltaic Single-Diode Model (PVSDM), Double Diode Model (PVDDM), and Triple- Diode Model (PVTDM) is demonstrated to consider the PV losses. This article introduces a new application of the Forensic-Based Investigation Algorithm (FBIA), which is a new meta-heuristic optimization technique, to accurately extract the electrical parameters of different PV models. The FBIA is inspired by the suspect investigation, location, and pursuit processes that are used by police officers. The FBIA has two phases, which are the investigation phase applying by the investigators team, and the pursuit phase employing by the police agents team. The validity of the FBIA for PVSDM, PVDDM, and PVTDM is commonly considered by the numerical analysis executing under diverse values of solar irradiations and temperatures. The optimal five, seven, and nine parameters of PVSDM, PVDDM, and PVTDM, respectively, are accomplished using the FBIA and compared with those manifested by various optimization techniques. The numerical results are compared for the marketable Photowatt-PWP 201 polycrystalline and Kyocera KC200GT modules. The efficacy of the FBIA for the three models is properly carried out checking its standard deviation error with that obtained from various recently proposed optimization techniques in 2020 which are Jellyfish search (JFS) optimizer, Manta Ray Foraging optimizer (MRFO), Marine Predators Algorithm(MPA), Equilibrium Optimizer (EO), Heap Based Optimizer (HBO). The standard deviations of the fitness values over 30 runs are developed to be less than 1×10^{-6} for the three models, which make the FBIA results are extremely consistent. Therefore, FBIA is foreseen to be a competitive technique for PV module parameter extraction.

INDEX TERMS PV parameters extraction, PV single-diode model, double diode model, triple- diode model forensic-based investigation algorithm, Kyocera KC200GT modules, Photowatt-PWP 201.

I. INTRODUCTION

Myriads of efforts have been developed to adjust the energy structure and increase renewable energy research in order to cope with the dramatically increasing of energy shortage and environment issues. There are many types of renewable energy technologies, however, solar photovoltaic is categorized to be the most feasible type to overcome the increasing in the energy demands. One of the most important issues of advancement of PV technology is the parameter extraction and accurate modeling which describe the nonlinear characteristics of current–voltage (I–V) of solar cells. These parameters extraction drew high consideration in simulation, assessment and maximum energy collected from the PV systems [1], [2]. Over the past decades, although numerous models have been developed to manifest the parameter equivalent circuit of solar cells, three lumped models are used practically, which are Photovoltaic Single-Diode Model (PVSDM), Double Diode Model (PVDDM), three Diode (PVDDM) Model [3], [4]. In these three models, there are five, seven, and nine parameters need to be extracted accurately.

The associate editor coordinating the review of this manuscript and approving it for publication was Pavlos I. Lazaridis.

Three popular methods, which are analytical, nonlinear optimization, metaheuristics methods, have been elaborated in the literature to estimate the unknown parameters of PV cells. The first one is the analytical methods that are utilized based on the data sheet information or I-V curve [5]–[7] to illustrate suitable estimation process formulations. Additionally, analytical expressions are presented in [8] to determine the parameters of the single-diode model at any operating conditions, whilst a novel three-terminal measurement technique is used with a Tandem structure to extract the essential solar sub-cells parameters [9]. An application of the direct extraction procedure for the measured I–V characteristics of an experimental organic solar cells is introduced in [10] displaying the analytic solution with the illumination intensity-dependent S-shapes. The second method is the nonlinear optimization methods in [11], [12]. These two approaches use sets of experimental data for estimating the unknown parameters of PV cells. The third method is the metaheuristic optimization methods, which are demonstrated to solve the optimization problem. In this context, A data-driven method [13], a modified simplified swarm optimization (MSSO) algorithm [14], and adaptive wind-driven optimization (AWDO) algorithm [15] are developed to extract I–V curve parameters of PVSDM. Accurate Expressions for PVSDM is proposed in [16] without any approximation. A reduced computational complexity via a Reduced-Space Search for PVSDM is introduced in [17]. An explicit nonlinear model, which uses per unit single-diode model of PV module [18], is proposed to determine the parameters of PVSDM. Two-step linear least-squares method is presented in [19] taking into consideration intrinsic properties of the model equation to extract the parameters of PVSDM. Other techniques such as Coyote Optimization Algorithm (COA) [20], evolutionary algorithms (EAs) [21] and an improved cuckoo search optimization (ICSO) [22] are presented to extract PVSDM and PVDDM. Additionally, Bacterial Foraging Optimization (BFO) [23] technique can extract the optimal parameters when changing the weather conditions. A triple-phase teaching-learning-based optimization (TPTLBO) [24], Coyote Optimization Algorithm (COA) [25], an interval branch and bound algorithm [26] Tree Growth Algorithm (TGA) [27], are applied to extract the parameters of different PV models of the three models. shuffled complex evolution (SCE) [28] technique was developed for only extracting the intrinsic parameters of the PVTDM. The marine predators' algorithm (MPA) [29] and Manta Ray Foraging (MRF) optimizer [30] are properly employed to extract the electrical parameters of the PVTDM for different PV Modules. A detailed overview of the solar cell models for a common PV panel was evaluated in [31], but only for PVSDM and PVDDM. In [32], a penalty based-differential evolution has been extended to the extraction of PVDDM module parameters under varying environmental conditions of various forms (mono-crystalline, multi-crystalline and thinfilm).

It is clearly observed that the previous survey illustrates the great effort that has been demonstrated to get the optimal parameters for each model. In this article, a fewer controlling parameter and an adequate time consumption approach named Forensic-Based Investigation Algorithm (FBIA) [33] is proposed to estimate the electrical parameters of PV modules. FBIA can be represented by the investigation stage employed by the investigators team, and the pursuit phase applied by the police agents' team to attain the fitness function. The quality of FBIA is assessed measuring the experimental datasets under diverse environmental conditions of temperature and radiation values with handling the parameters of PVSDM, PVDDM and PVTDM models.

These three models are utilized with, two sets of I-V data—namely, the measurements attained from the Photowatt-PWP 201 polycrystalline module and the KC200 [34]. These datasets are selected because they are widely employed as benchmarks to assess the performances of several parameter extraction methods [35]–[37]. The exact value of each points and the best results attained by other methods in the literature. Therefore, these case studies provide fair, wide-reaching, and referenceable comparisons. The proposed algorithm is compared with a recent and a well-established algorithm to illustrate its superiority and effectiveness among these algorithms

It is lucid that the previous survey illustrate that a great effort has been demonstrated to get the optimal parameters for each model. Therefore, the noticed features of this article can be described in the following points:

- A novel optimization technique called FBIA is introduced and tested for estimating the parameters for single, double and triple models of PV cells with two different PV modules.
- The Photowatt-PWP 201 polycrystalline module is emulated via PVTDM model as a practical test solar cell for the first time in this article.
- The simulation results are compared with many algorithms in the literature when using the same data set.
- To prove the proposed new algorithm ability, many recent algorithms for the first time as Jellyfish search (JFS) optimizer [38], Manta Ray Foraging optimizer (MRFO) [39], [40], Marine Predator Algorithm (MPA) [41], Equilibrium Optimizer (EO) [42], [43], and Heap Based Optimizer (HBO) [44] are implemented in this work for the two modules.
- The performance of the proposed FBIA algorithm is inspected in terms of fitness value and convergence speed in comparison to other metaheuristics.
- The estimated characteristics of the selected PV cell are used to simulate both I-V curve and P-V curve, and they are nearly close to the experimental data.
- The FBIA is assessed with the measured experimental datasets under diverse environmental conditions of temperature and radiation values with handling the parameters of PVSDM, PVDDM and PVTDM models.

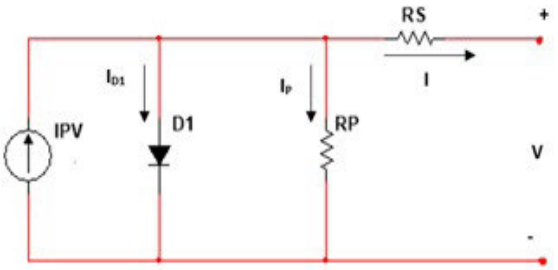

FIGURE 1. Equivalent circuit for PVSDM.

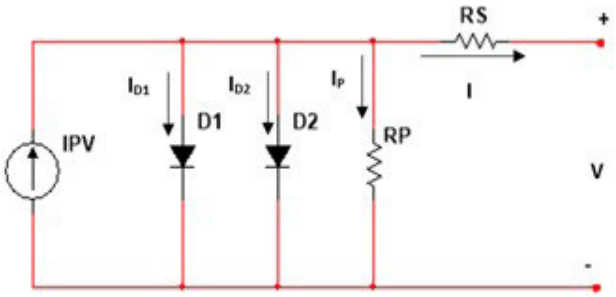

FIGURE 2. Equivalent circuit for PVDDM.

The paper is arranged in 5 section as follows: The problem formulation for different three PV models are detailed in Section II. Then, Section III demonstrates the steps to FBIA optimization algorithm. The outcomes are discussed and analyzed in Section VI with comparison and convergence analyses compared with the recently developed state-of-the art in literature. Eventually, a conclusion is manifested in Section V.

II. PROBLEM FORMULATION

A. SOLAR CELL MODELS

The characteristics of the PV have been explored by various models. Practically, the most popular ones are PVSDM, PVDDM, and PVTDM. The output current (I) of the PV cell is calculated from the output voltage (V) in the three models. Each model is manifested by an equivalent circuit with defined operating conditions. Additionally, the entire I − V curve of a module is considered as a continuous function. Furthermore, the temperature and the irradiance are fixed parameters and can influence on these models. Eventually, it is required to estimate the simplified inner characteristics of the PV models depending on the selected model.

The succeeding subsections describe the three model alternatives for PV cells.

1) PHOTOVOLTAIC SINGLE-DIODE MODEL (PVSDM)

In Fig. 1, the equivalent circuit of the PVSDM is displayed It consists of the photo-current source (IPV), the resistance (RP), that is shunted with the diode and a series resistance (RS). RP considers the leakage current of PN junction that involves the semiconductor non-idealities. It arises from the partial short circuit current path close to the cell's edges. Additionally, RS emulates the effects of contact surfaces of electrodes and silicon, and the passing current resistance, and electrodes resistance.

The PVSDM is formulated mathematically to calculate the load output current (I) as follows:

$$I = I_{PV} - I_{D1} - I_P \tag{1}$$

where, I_{PV}, I_{D1}, and I_P represent the photons current, the diode current, and the current, which passes throughout the shunt resistance, respectively.

I_{D1} can be formulated as:

$$I_{D1} = I_{S1}\left[\exp\left(\frac{V + IR_S}{\eta_1 V_T}\right) - 1\right] \tag{2}$$

where, I_{S1}, I manifest the reverse saturation current and the output current of the cell, respectively, whereas V, R_S and η_1 refer to the output voltage of the PV cell, the series resistance of the PVSDM equivalent circuit, and the ideality factor of $D1$, respectively.

Moreover, I_P is computed as:

$$I_P = \frac{V + IR_S}{R_P} \tag{3}$$

The constant V_T is calculated as follows:

$$V_T = \frac{K_B T}{q} \tag{4}$$

where, K_B describes the Boltzmann's constant, whilst T and q characterize the absolute temperature and the electron's charge, respectively. Consequently, the unknown parameters of the PVSDM become five which are I_{PV}, I_{S1}, η_1, R_P and R_S.

2) PHOTOVOLTAIC DOUBLE -DIODE MODEL (PVDDM)

In practical conditions, for the PVDDM, an additional diode is placed in parallel with the current source considering the recombination of space charge [31] in comparison with the PVSDM. The equivalent circuit of the PVDDM is illustrated in Fig. 2. The additional diode reflects the additional current term as depicted in the Eq. (5) as:

$$I = I_{PV} - I_{D1} - I_{D2} - I_P \tag{5}$$

where, I_{D2} gives the second diode current and can be described with the following equation:

$$I_{D2} = I_{S2}\left[\exp\left(\frac{V + IR_S}{\eta_2 V_T}\right) - 1\right] \tag{6}$$

where, I_{S2} shows the reverse saturation current, while η_2 represents the ideality factor of $D2$.

There are two extra parameters with respect to the second model, PVSDM, describing the second diode. Therefore, the PVDDM will have seven unknown parameters that are I_{PV}, I_{S1}, I_{S2}, η_1, η_2, R_P and R_S.

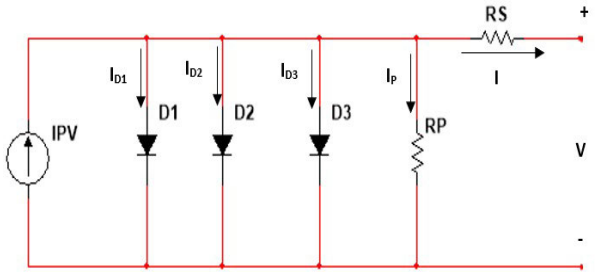

FIGURE 3. Equivalent circuit for PVTDM.

3) PHOTOVOLTAIC TRIPLE -DIODE MODEL (PVTDM)

In this model, the impact of large leakage and recombination in the defect area are considered. Thus, the third diode is shunted with the PVDDM as depicted in Fig. 3.

Like PVSDM and PVDDM, the output current is computed by employing Kirchhoff current law as depicted in the following equation:

$$I = I_{PV} - I_{D1} - I_{D2} - I_{D3} - I_P \tag{7}$$

where, the third diode current (I_{D3}) can be calculated as follows:

$$I_{D3} = I_{S3}\left[\exp\left(\frac{V + IR_S}{\eta_3 V_T}\right) - 1\right] \tag{8}$$

where, I_{S3} describes the reverse saturation current, whereas η_3 reflects the ideality factor of $D3$.

In the previous methods [45]–[47], only seven parameters, which are I_{PV}, I_{S1}, I_{S2}, I_{S3}, η_3, R_P and R_S, are estimated, whilst the other parameters remain constants $\eta_1 = 1$, $\eta_2 = 2$ and only an additional constraint is added, which is $\eta_3 > 3$. However, in this article, the nine parameters of PVTDM have been examined with different recently developed optimization techniques to augment the accuracy of the model.

4) OBJECTIVE FUNCTION FORMULATION

It is pivotal to define firstly an appropriate objective function in order to effectively apply FBIA for the PV parameter extraction problem. The main objective of PVSDM, PVDDM, and PVTDM is to find their parameter values that can minimize the errors between both calculated and measured current. Basically, the greatest accurate group of model parameters should be slightly more or less than the experimental data. In that context, the broadly accepted scheme, to measure the difference between two I-V curves, is developed throughout the root mean square error (RMSE) [20]. Hence, the objective function can be determined as [48]–[50] as:

$$RMSE = \sqrt{\frac{1}{M}\sum_{j=1}^{M}(I_{exp}^{j} - I_{cal}^{j}(V_{exp}^{j}, x))^2} \tag{9}$$

where, I_{exp}^{j} and V_{exp}^{j} illustrate the current and voltage values of j^{th} experimental point, respectively, while N describes the number of empirical data points. The variable x indicates the decision parameters of the optimization problem. On the contrary, the term (I_{cal}^{j} ($V_{\exp}^{j}$, x)) represents the computed current output.

III. FBIA FOR OPTIMIZED PARAMETERS EXTRACTION OF SOLAR CELL MODELS

The FBIA, introduced by Chou and Nguyen, is influenced by the forensic examination techniques of police officers. The FBIA is stimulated by police personnel who use the investigation, location, and conviction of criminals. The FBIA has two main phases, which are the investigation phase and the pursuit phase. While the investigation phase is applied by the investigators team, the pursuit phase is employed by the police agents' team.

X_{Ai} represents the i_{th} suspected place to be investigated during the inquiry process; ($i = 1, 2, \ldots, NPA$); Whereas X_{Bi} indicates the position of the police officer i at which police officer continues to pursue the perpetrator, ($i = 1, 2, \ldots, NPB$). NPA and NPB are related to the pursuit team which describe the places number that are inspected and police agents, respectively. The size of population (NP), in this algorithm, is assumed to equal to NPA and NPB. Whenever the full number of iterations ($gmax$) is completed, the forensic process is terminated. Its main steps are depicted in Fig. 4.

The algorithm consists of four steps which are interpretation of findings (A1), direction of inquiry (A2), actions (B1) and extends the process of actions (B2) as will be illustrated in the following paragraphs.

In (A1), a new suspected location (X_{A1i}) from X_{Ai} is deduced on the basis of X_{Ai} and information, which is related to other suspected locations. It is assumed that each individual moves underneath the effect of other individuals. Thus, the movement formula can be expressed as seen in the following equation:

$$X_{A1_{ij}} = X_{A_{ij}} + ((r - .05) * 2) * \left(\sum_{a=1}^{a_1} X_{A_{aj}}\right)/a_1, \quad a_1 \in \{1, 2, \ldots, n-1\} \tag{10}$$

where $j = 1$: D and D indicates the dimensions number, whilst the term ((r − 0.5)*2) and the symbols (r) and (a) represent a random number in the range [−1, 1] and [0, 1], respectively, a_1 denotes the number of individuals which affect the movement of X_{Aij}. The updated suspected place X_{A1i} is shown in Eq. (11). p_{Ai} is considered as the possibility that the suspect is located at X_{Ai}, which means that p_{Ai} represents the objective value of location X_{Ai}. The investigators assess the possibility (p_{A1i}) of the new place for suspect in comparison to the existed one based on the objective value to reserve the better one.

$$X_{A1_{ij}} = X_{A_{ij}} + ((r_1 - .5) * 2) * (X_{A_{ij}} - (X_{A_{kj}} + X_{A_{hj}})/2), \quad \{k, h, i\} \in \{1, 2, \ldots, NP\} \tag{11}$$

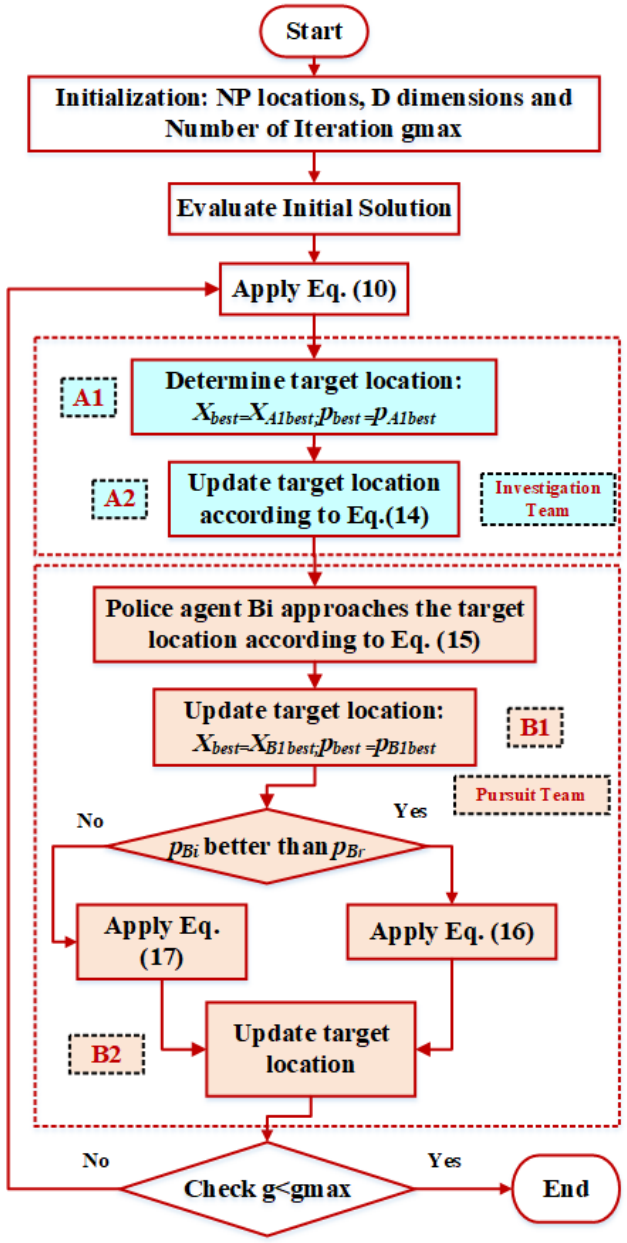

FIGURE 4. Main steps of FBIA.

whereas, h and k indicate random selected places and i refer to the current place D and NP are the dimensions number and the locations number for suspect, respectively. Additionally, the term $((r_1 - 0.5)^*2)$ and (r_1) characterize random numbers within ranges $[-1, 1]$, and $[0, 1]$, respectively.

In (A2),investigators direct the inquiry. p_{worst} represents the lowest possibility, which is the worst objective value, whereas p_{best} *and* X_{best} are the highest possibility (the best objective value) and the best location, respectively. The probability of each location ($Prob(X_{Ai})$) can be determined and consequently, a high probability for the location $Prob(X_{Ai})$ that equals:

$$\Pr ob(X_{A_i}) = (p_{worst} - p_{A_i})/(p_{worst} - p_{best}) \quad (12)$$

TABLE 1. The boundaries range for Photowatt-PWP 201 moduleparameters [36].

Parameter	Lower bound	Upper bound
I_{ph} (A)	0	2
I_{sd}, Isd1, Isd2 (μA)	0	50
R_S (Ω)	0	2
R_{sh} (Ω)	0	2000
n, n_1, n_2	1	50

Based on the steps A1 and A2, Thus, the formula of the movement can be expressed as depicted in the following equation

$$X_{A2_i} = X_{best} + \sum_{b=1}^{a_2} \alpha_b * X_{A_{bj}} \quad a_2 \in \{1, 2, \ldots, n-1\} \quad (13)$$

where, X_{best} expresses the best location; a_2 represents the number of individuals which affect the move of X_{A2i}; $b = 1, 2, \ldots, a_2$; α_b displays the effectiveness coefficient of the other individuals to the move and it is within the range $[-1, 1]$). Numerical experiments indicate that $a_2 = 3$. Therefore, the new suspected location X_{A2ij} is created using Eq. (14). Then, the possibility (objective) is computed to decide updating the suspected place or not.

$$X_{A2_{ij}} = X_{best} + X_{A_{dj}} + r_5 * (X_{A_{ej}} - X_{A_{fi}}) \{f, d, i, e\} \in \{1, 2, \ldots, NP\} \quad (14)$$

where X_{best} describes the best place and r_5 represents the random value between 0 and 1, while e, d, i, and f, denote four suspected locations.

In Step (B1), every B_i agent is approaching the position that has the highest value of the objective as illustrated in Eq. (15). Then, the new position is changed if it finds a better fitness compared to the existed one (p_{Bi}).

$$X_{B1_{ij}} = r_6 * X_{B_{ij}} + r_7 * (X_{best} - X_{B_{ij}}) \quad j = 1, 2, \ldots, D \quad (15)$$

where X_{best} displays the best place provided by the investigators, while r_6 and r_7 describe numbers that are randomly specified inside [0, 1].

In Step (B2), each agent B_i coordinates with the others, and B_i shifts in the direction of the best place. The updated position (X_{B2i}) of the agent B_i is formalized as manifested in Eq. (16) if the possibility (p_{Br}) of another member B_r is better than p_{Bi}; Otherwise, it is computed as illustrated in Eq. (17).

$$X_{B2_{ij}} = X_{B_{rj}} + r_8 * (X_{B_{rj}} - X_{B_{ij}}) + r_9 * (X_{best} - X_{B_{rj}}) \{i, r\} \in \{1, 2, \ldots, NP\} \text{ and } j = 1, 2, \ldots, D \quad (16)$$

$$X_{B2_{ij}} = X_{B_{ij}} + r_{10} * (X_{B_{ij}} - X_{B_{rj}}) + r_{11} * (X_{best} - X_{B_{ij}}), \{i, r\} \in \{1, 2, \ldots, NP\} \text{ and } j = 1, 2, \ldots, D \quad (17)$$

where X_{best} describes the best location given in *Step B1*, while (r_8),(r_9),(r_{10}), and (r_{11}) are random numbers within the range [0, 1]. The two symbols(i) and (r) reflects two police agents, and r is selected randomly.

TABLE 2. The Min, Mean, Max and Std of both recent and reported optmization techniques on PVSDM of PWP 201 polycrystalline Module.

	PSO [51]	GWO [52]	PSOGWO [53]	SMA [54]	RAO [55]	CS [56]	EO	HEAP	JFS	MPA	MRFO	FBIA
min	0.002439	0.003816	0.003891	0.002811	0.002822	0.002826	0.002425	0.002426	0.002425	0.002437	0.002425	0.002425
mean	0.023666	0.009582	0.006287	0.003353	0.003296	0.003745	0.002439	0.002455	0.002427	0.003686	0.002432	0.002426
max	0.09770	0.016896	0.01033	0.010799	0.425535	0.576412	0.002528	0.00252	0.002434	0.015104	0.002506	0.002435
Std	4.16E− 2	6.11E− 3	2.65E− 3	6.25E-03	9.84 E-3	1.64E-02	2.75E-5	2.42E-5	2.37E-6	3.13E-3	1.58E-5	2.02E-6
Time/Iteration (Sec)	NR	NR	NR	NR	NR	NR	0.08592	0.09257	0.08876	0.08291	0.082004	0.076966

NR indicates not reported

TABLE 3. Parameter estimation extracted of both recent and reported optmization techniques on PVSDM of PWP 201 polycrystalline Module.

Para-meters	PSO [51]	GWO [52]	PSOGWO [53]	SMA [54]	RAO [55]	CS [56]	EO	HEAP	JFS	MPA	MRFO	FBIA
Iph	1.0343	1.0316	1.0306	1.03422	1.03426	1.03536	1.030451	1.030337	1.030513	1.030082	1.030517	1.030512
Rs	0.0366	0.0312	0.0291	1.25644	1.30421	1.23635	0.033358	0.033285	0.033369	0.033534	0.033369	0.033367
Rsh	15.1951	18.6488	40.8095	15.5403	15.4041	15.3086	27.51263	28.218	27.26045	28.20094	27.27375	27.29215
Io	1.23E-6	4.42E-6	9.08E-06	1.32E-06	1.37E-06	2.31E-06	3.5E-06	3.59E-06	3.48E-06	3.34E-06	3.48E-06	3.48E-06
n	1.3332	1.4713	1.5610	45.19925	47.08478	48.97456	1.351632	1.354297	1.351138	1.346571	1.35119	1.351247

TABLE 4. Parameter estimation extracted of additionl reported optmization techniques on PVSDM of PWP 201 polycrystalline Module.

Para-meters	JAYA [57]	PGJAYA [58]	TLABC [59]	STLBO [60]	CMM-BBO [61]	EHA-NMS [62]	ITLBO [63]	SATLBO [64]	GWOCS [65]	HFAPS [66]	ALO [67]
Iph	1.03020	1.03050	1.03050	1.03050	1.03050	1.03051	1.03050	1.03051	1.03049	1.03050	1.03166
Rs	0.03337	0.03337	0.03337	0.03337	0.03337	0.03337	0.03337	0.03337	0.03339	0.03337	0.03038
Rsh	28.403	27.274	27.282	27.278	20.964	27.277	27.288	27.299	27.299	27.341	11.248
Io	3.49 E-6	3.48 E-6	3.48 E-6	3.48 E-6	3.48 E-6	3.48 E-6	3.48 E-6	3.48 E-6	3.47 E-6	3.48 E-6	4.52E-6
n	1.3514	1.3512	1.3512	1.3512	1.3512	1.3512	1.3512	1.3512	1.3507	1.3512	1.3831
min	0.0024278	0.0024251	0.0024251	0.0024251	0.0024251	0.0024250	0.0024251	0.0024251	0.0024251	0.0024251	0.00280
mean	0.0024537	0.0024251	0.0024255	0.020553	0.0024259	0.0024251	0.0024251	-	0.0024261	-	-
max	0.0025959	0.0024268	0.0024287	0.2742508	0.0024268	0.0024251	0.0024251	-	0.0024275	-	-

IV. SIMULATION RESULTS

In this section, FBIA is employed on the Photowatt-PWP 201 polycrystalline module and Kyocera KC200GT module to extract the electrical PVSDM, PVDDM, and PVTDM parameters accurately.

A. PHOTO WATT-PWP 201 PV MODULE

The first test system, which is Photo watt-PWP 201 PV Module, has 36 series polycrystalline silicon cells that were tested to get the measured data which consists 25 pairs of I and V values at an irradiance of (1000 W/m^2) and a temperature of (45 °C) [34]. The parameters search ranges are set according to other related works [35], [36], as depicted in Table 1. The three-model system, which are PVSDM, PVDDM, and PVTDM are illustrated below as follows.

1) CASE 1: PVSDM

For this case, FBIA is employed on, where the optimal solution, which is the minimum error, is compared with respect to those manifested by various reported and recently developed optimization techniques as shown in Table 2. The stopping criteria is reached when the maximum number of iterations (gmax) of 2000 is achieved. On the one hand, it is apparently seen that the FBIA and finds a minimum standard deviation of 2.02E-06, which is lower than EO, HEAP, JFS, MPA, and MRFO, where they acquired Std of 2.75E-05, 2.42E-05, 2.37E-06, 0.003134, 1.58E-05, and 2.02E-06, respectively. Added to that, the computational cost of the executed time per each iteration are compared for the performed algorithms. As shown, the lower computational cost is related to FBIA with 0.076966 seconds whilst, EO, HEAP, JFS, MPA and MRFO records 0.08592, 0.09257, 0.08876, 0.08291 and 0.082004 seconds.

In addition, Tables 3 and 4 illustrate the parameter estimation extracted of both recent and reported optimization techniques on PVSDM of PWP 201 polycrystalline Module. The reported optimization techniques, that are employed in this study, are particle swarm optimization (PSO) [51], grey wolf optimization (GWO) [52], particle swarm optimization based grey wolf optimization (PSOGWO) [53], slime mould optimization (SMA) [54], RAO optimizer [55], CS [56], JAYA Algorithm [57], performance-guided JAYA (PGJAYA) [58], teaching–learning–based artificial bee colony (TLABC) [59], simplified TLBO (STLBO) [60], covariance matrix based migration with biogeography- based optimization (CMM-BBO) [61], eagle based hybrid adaptive Neld-Mead simplex (EHA-NMS) [62], improved teaching learning based optimization (ITLBO) [63], self-adaptive TLBO (SATLBO)

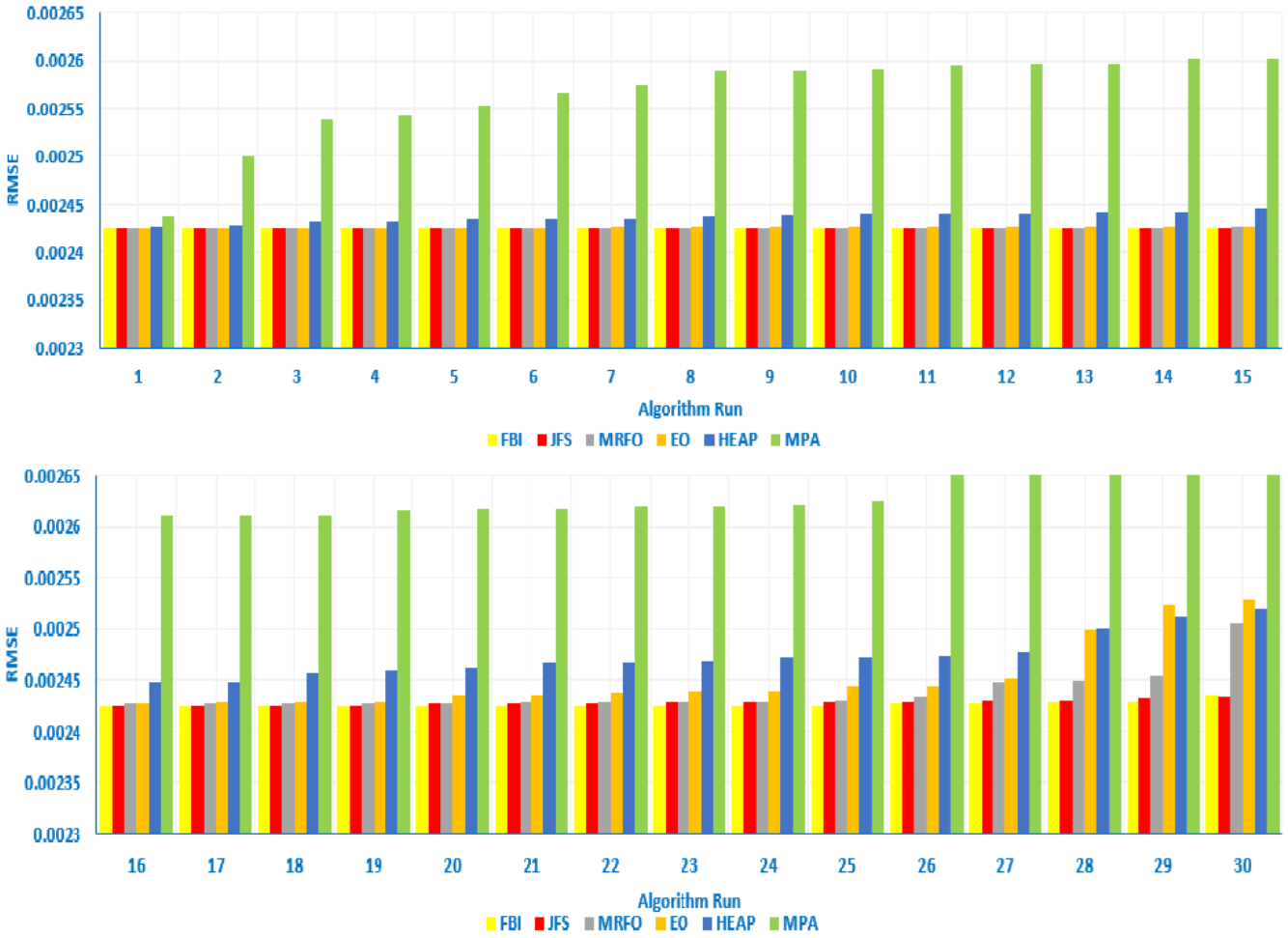

FIGURE 5. RMSE of FBIA compared to recent optmization techniques on PVSDM of PWP 201 polycrystalline Module.

[64], grey wolf optimizer with cuckoo search (GWOCS) [65], hybrid Firefly and Pattern Search (HFAPS) [66], and Ant lion optimizer (ALO) [67].

Fig. 5 displays the RMSE of FBIA compared to recent optmization techniques, which are JFS, MRFO, HEAP, EO, MPA on PVSDM of PWP 201 polycrystalline Module. The RMSE data were obtained depending on 30 Runs for all recent algorithms. Fig. 5 illustrtaes that the proposed FBIA achives the lowest RMSE value among the recently developed techniques in the literature where the RMSE value for FBIA accounts for 0.002425 in the 30 run processes. Therefore, the convergence characteristics of the FBIA are stable and the arrival of the optimal solution is faster than the other recent optmization techniques depicting in Fig. 6.

Figs. 7 and 8 illustrate the simulated behavior of the PV using the MSD result compared with respect to the data that used for the parameter estimation. The current–voltage (I–V) and the power-voltage (P-V) curves of the PV are depicted in Fig. 7 and Fig. 8, respectively.

Table 5 illustrates the points of experimental, simulated current values, and the absolute errors between them.

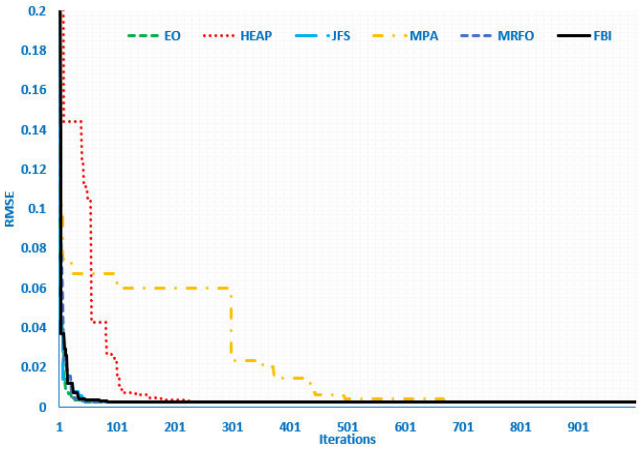

FIGURE 6. Convergence charactrictics of FBIA versus other recent optmization techniques on PVSDM of PWP 201 polycrystalline.

Moreover, it manifests the experimental, simulated power values, and the absolute errors between them when employing the FBIA on PVSDM of PWP 201 polycrystalline.

TABLE 5. Experimental and simulated current and power of FBIA on PVSDM of PWP 201 polycrystalline and the absolute errors among them.

Vexp	Iexp	Isim	Pexp	Psim	IAE	PAE	Absolut IAE	Absolut PAE
0.1248	1.0315	1.029118	0.128731	0.128434	-0.00238	0.000297	0.002382482	0.000297334
1.8093	1.03	1.02738	1.863579	1.858839	-0.00262	0.00474	0.002619646	0.004739726
3.3511	1.026	1.025742	3.438229	3.437364	-0.00026	0.000865	0.000258095	0.000864903
4.7622	1.022	1.024108	4.866968	4.877007	0.002108	-0.01004	0.002107983	0.010038638
6.0538	1.018	1.022293	6.162768	6.188759	0.004293	-0.02599	0.004293221	0.025990301
7.2364	1.0155	1.019933	7.348564	7.38064	0.004433	-0.03208	0.004432507	0.032075395
8.3189	1.014	1.016365	8.435365	8.45504	0.002365	-0.01968	0.002365099	0.019675021
9.3097	1.01	1.010498	9.402797	9.407433	0.000498	-0.00464	0.000497995	0.00463618
10.2163	1.0035	1.00063	10.25206	10.22274	-0.00287	0.029318	0.002869711	0.029317827
11.0449	0.988	0.984549	10.91236	10.87424	-0.00345	0.038118	0.003451203	0.03811819
11.8018	0.963	0.959521	11.36513	11.32407	-0.00348	0.04106	0.003479103	0.041059677
12.4929	0.9255	0.922837	11.56218	11.52891	-0.00266	0.033272	0.002663284	0.033272142
13.1231	0.8725	0.872596	11.4499	11.45117	9.63E-05	-0.00126	9.63364E-05	0.001264233
13.6983	0.8075	0.80727	11.06138	11.05823	-0.00023	0.00315	0.000229962	0.003150095
14.2221	0.7265	0.728332	10.33236	10.35841	0.001832	-0.02605	0.001831782	0.026051784
14.6995	0.6345	0.637133	9.326833	9.365541	0.002633	-0.03871	0.002633287	0.038707998
15.1346	0.5345	0.536209	8.089444	8.115304	0.001709	-0.02586	0.001708706	0.025860583
15.5311	0.4275	0.429507	6.639545	6.670724	0.002007	-0.03118	0.002007492	0.031178555
15.8929	0.3185	0.318771	5.061889	5.066199	0.000271	-0.00431	0.000271242	0.004310824
16.2229	0.2085	0.207387	3.382475	3.364414	-0.00111	0.01806	0.001113267	0.018060411
16.5241	0.101	0.096165	1.668934	1.589035	-0.00484	0.079899	0.00483528	0.079898643
16.7987	-0.008	-0.00833	-0.13439	-0.1399	-0.00033	0.005511	0.000328073	0.005511194
17.0499	-0.111	-0.11094	-1.89254	-1.89151	6.04E-05	-0.00103	6.04156E-05	0.00103008
17.2793	-0.209	-0.20925	-3.61137	-3.61571	-0.00025	0.004338	0.000251064	0.004338202
17.4885	-0.303	-0.30087	-5.29902	-5.26174	0.002132	-0.03728	0.002131534	0.037277339

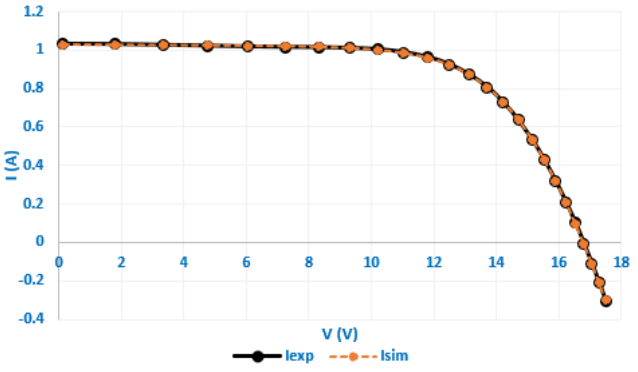

FIGURE 7. I-V curve of experimental and simulated current of FBIA on PVSDM of PWP 201 polycrystalline.

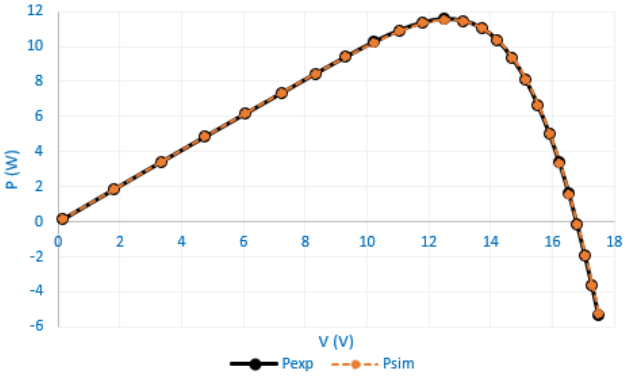

FIGURE 8. P-V curve of experimental and simulated current of FBIA on PVSDM of PWP 201 polycrystalline.

In addition, Figs. 9 and 10 demonstrate the absolute errors of experimental and simulated current of FBIA on PVSDM of PWP 201 polycrystalline module when applying 25 runs according to the standard of the module benchmark.

2) CASE2: PVDDM

FBIA is employed on PVDDM, in this case, where the optimal solution is compared with respect to the other optimization techniques in Table 6. It is clearly seen that the FBIA finds a minimum standard deviation of 4.75E-06, which is less than EO, HEAP, JFs, MPA, and MRFO, where they acquired Std of 9.14E-06, 2.52E-05, 5.25E-06, 0.000704, 1.36E-05, and 1.36E-05, respectively. Table 7 characterizes the parameter estimation extracted from the recent and reported optimization techniques on PVDDM of PWP 201 polycrystalline module, where the proposed FBIA achieves the most accurate results for these parameters with respect to the other techniques. Table 6 also manifests the parameter estimation extracted of reported optimization techniques on PVSDM of PWP 201 polycrystalline module, which are particle swarm optimization (PSO) [51], grey wolf optimization (GWO) [50], Lightning Attachment Procedure Optimization (LAPO) [66] particle swarm optimization based grey wolf optimization (PSOGWO) [51].

Fig. 11 illustrates the RMSE of FBIA compared to the recent optmization techniques, which are JFS, MRFO, HEAP, EO, MPA on PVDDM of PWP 201 polycrystalline Module. The RMSE data were obtained depending on 30 Runs for all recent algorithms. It is seen that the proposed FBIA achives the lowest RMSE value among the recently developed techniques in the literature where the RMSE value and the

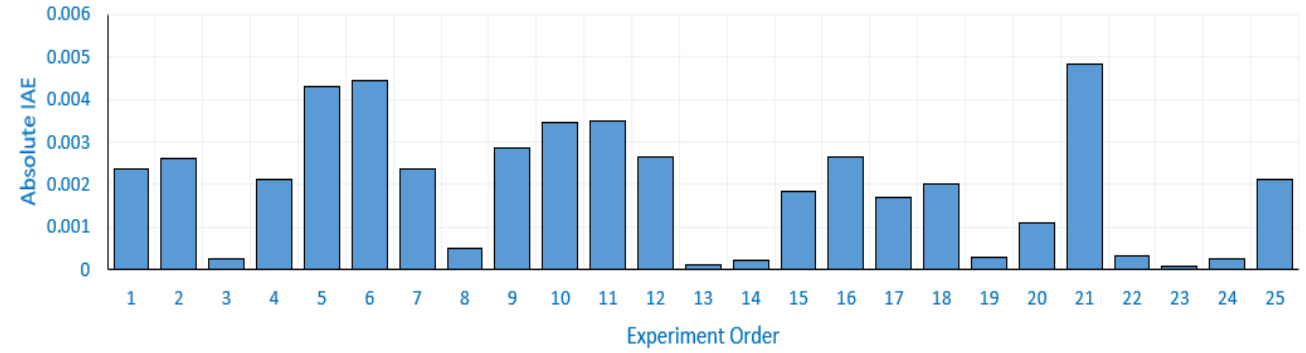

FIGURE 9. The absolute errors of experimental and simulated current of FBIA on PVSDM of PWP 201 polycrystalline.

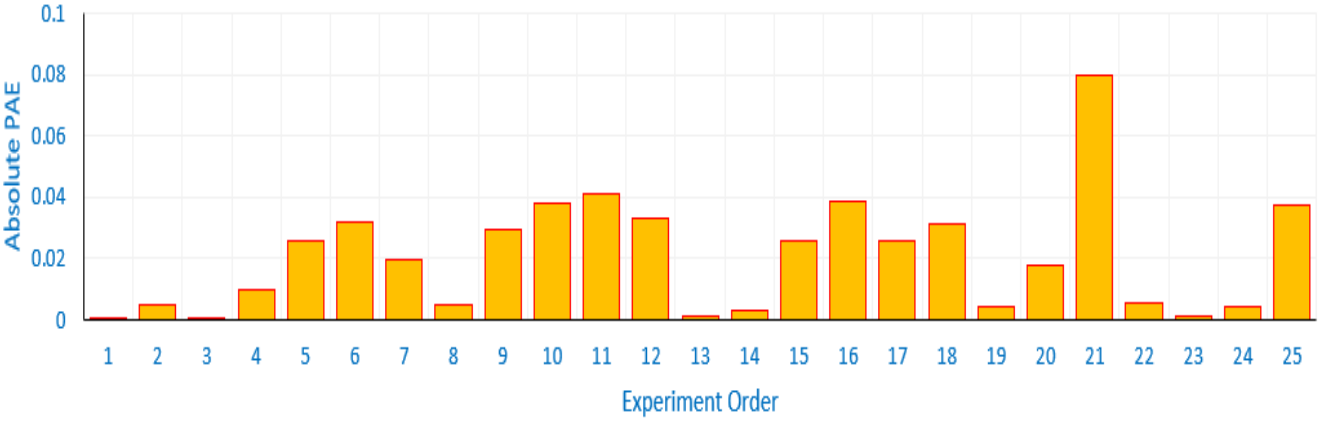

FIGURE 10. The absolute errors of experimental and simulated power of FBIA on PVSDM of PWP 201 polycrystalline.

TABLE 6. The Min, Mean, Max and Std of both recent and reported optmization techniques on PVDDM of PWP 201 polycrystalline Module.

	PSO [51]	GWO [52]	LAPO [68]	PSOGWO [53]	EO	HEAP	JFS	MPA	MRFO	FBIA
min	0.0033925	0.0055068	0.032734	0.0041674	0.002425	0.002428	0.002426	0.002505	0.002425	0.002425
mean	0.020808	0.081767	0.043132	0.077141	0.002434	0.002473	0.002434	0.002762	0.002435	0.002431
max	0.033742	0.10093	0.057507	0.10063	0.002453	0.00252	0.002443	0.006264	0.002492	0.002443
Std	1.59E− 2	4.26E− 2	9.14E− 3	4.18E− 2	9.14E-06	2.52E-05	5.25E-06	0.000704	1.36E-05	4.75E-06

TABLE 7. Parameter estimation extracted from of both recent and reported optmization techniques on PVDDM of PWP 201 polycrystalline Module.

Parameters	PSO [51]	GWO [52]	LAPO [68]	PSOGWO [53]	EO	HEAP	MPA	MRFO	JFS	FBIA
Iph	1.0291	1.0317	0.9801	1.0317	1.03054	1.030409	1.030354	1.030512	1.030293	1.030538
Rs	0.0314	0.0350	0.0396	0.0316	0.033375	0.033326	0.032728	0.033373	0.033339	0.033358
Rsh	75.6531	14.5388	73.0393	81.3713	27.17874	28.33547	30.53537	27.2848	28.17502	27.26848
Io1	1 E-09	8.37E-8	8.4 E-9	1 E-09	1.04E-06	3.56E-06	2.62E-12	3.31E-06	2.35E-06	2.88E-06
n1	1.0000	1.1528	1.0000	1.0000	1.351035	1.353583	1.067697	1.351032	1.356141	1.350415
Io2	9.38E-6	9.58E-6	8.09E-8	10 E-06	2.44E-06	0	4.25E-06	1.7E-07	1.19E-06	6.01E-07
n2	1.5755	1.6944	1.2000	1.5845	1.35097	1.354422	1.372776	1.35194	1.346628	1.356549

standard deviation of FBIA accounts for 0.002425 and 4.75E-06, respectively, in the 30 run processes. Then, the convergence characteristics of the FBIA are stable and the arrival of the optimal solution is faster than the other recent optmization techniques in Fig. 12.

Figs. 13 and 14 manifest the simulated behavior of the PVDDM result compared with respect to the data for the parameter estimation. The two figures show he current–voltage (I–V) and the power-voltage (P-V) curves of the PVDDM.

Table 8 gives the points of experimental, simulated current values, and the absolute errors between them. Moreover, it manifests the experimental, simulated power values and the absolute errors between them when employing

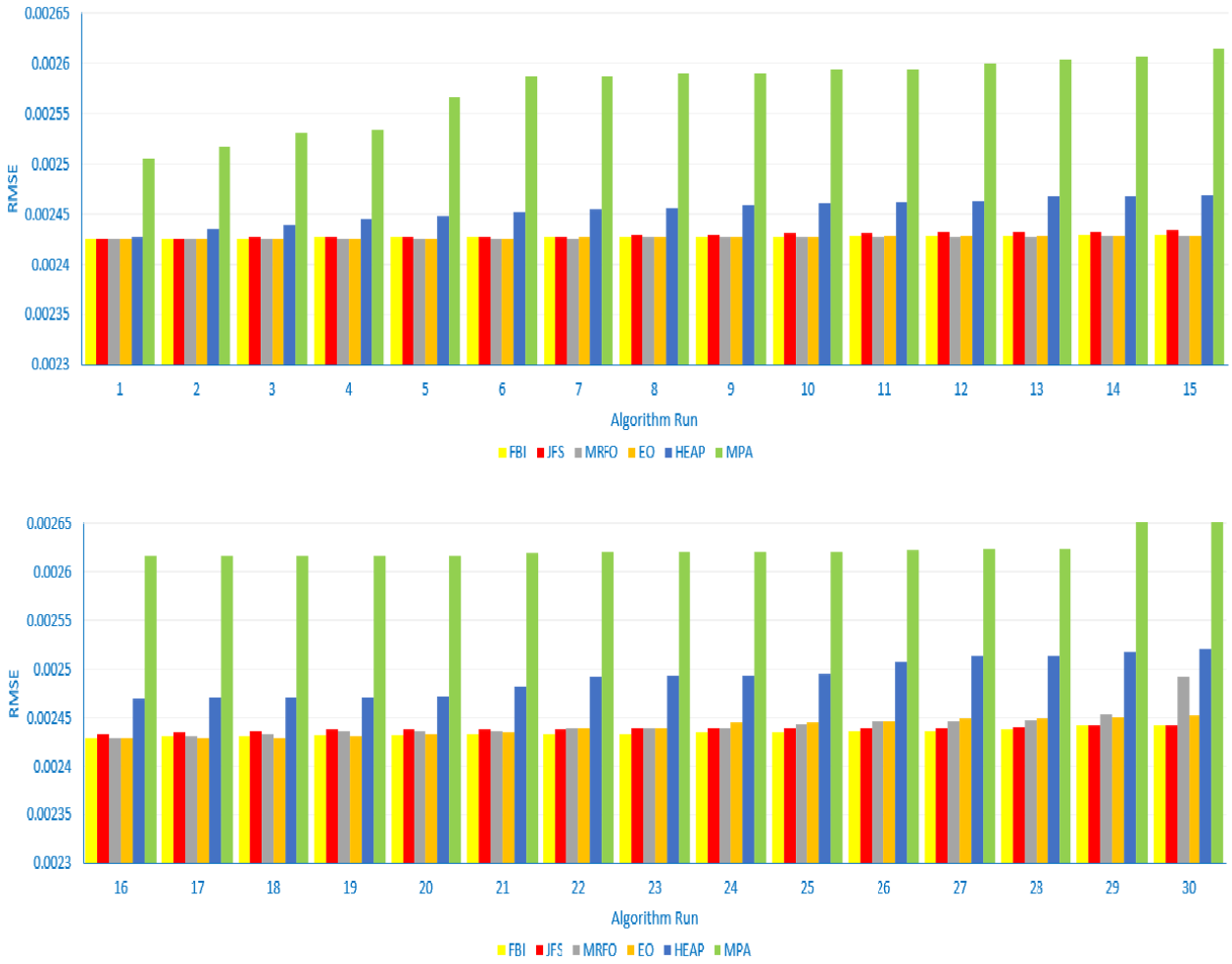

FIGURE 11. RMSE of FBIA compared to recent optmization techniques on PVDDM of PWP 201 polycrystalline Module.

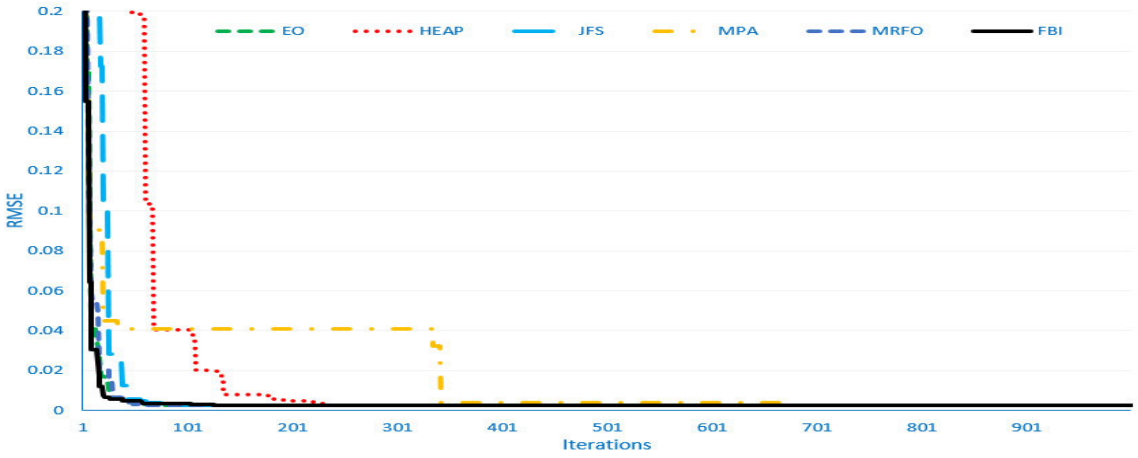

FIGURE 12. Convergence charactrictics of FBIA versus other recent optmization techniques on PVDDM of PWP 201 polycrystalline.

the FBIA on PVSDM of PWP 201 polycrystalline. In addition, Figs. 15 and 16 demonstrate the absolute errors of experimental and simulated current of FBIA on PVSDM of PWP 201 polycrystalline module when applying 25 runs according to the standard of the module benchmark.

TABLE 8. Experimental and simulated current and power of FBIA on PVSDM of PWP 201 polycrystalline and the absolute errors among them.

Vexp	Iexp	Isim	Pexp	Psim	IAE	PAE	Absolut IAE	Absolut PAE
0.1248	1.0315	1.02914	0.128731	0.128437	-0.00236	0.000294	0.002359703	0.000294491
1.8093	1.03	1.027403	1.863579	1.858881	-0.0026	0.004698	0.00259674	0.004698282
3.3511	1.026	1.025765	3.438229	3.43744	-0.00024	0.000789	0.000235308	0.000788541
4.7622	1.022	1.02413	4.866968	4.877113	0.00213	-0.01014	0.002130157	0.010144234
6.0538	1.018	1.022314	6.162768	6.188884	0.004314	-0.02612	0.004313859	0.026115241
7.2364	1.0155	1.01995	7.348564	7.380767	0.00445	-0.0322	0.004450057	0.032202389
8.3189	1.014	1.016377	8.435365	8.455141	0.002377	-0.01978	0.002377241	0.019776028
9.3097	1.01	1.010502	9.402797	9.407468	0.000502	-0.00467	0.000501756	0.004671197
10.2163	1.0035	1.000623	10.25206	10.22266	-0.00288	0.029397	0.002877434	0.029396728
11.0449	0.988	0.984527	10.91236	10.87401	-0.00347	0.038354	0.003472574	0.038354231
11.8018	0.963	0.959486	11.36513	11.32366	-0.00351	0.041472	0.003514009	0.041471626
12.4929	0.9255	0.922792	11.56218	11.52835	-0.00271	0.033834	0.002708219	0.033833504
13.1231	0.8725	0.872548	11.4499	11.45054	4.82E-05	-0.00063	4.82193E-05	0.000632787
13.6983	0.8075	0.807228	11.06138	11.05766	-0.00027	0.00372	0.000271554	0.003719823
14.2221	0.7265	0.728305	10.33236	10.35803	0.001805	-0.02568	0.001805423	0.025676911
14.6995	0.6345	0.637129	9.326833	9.365477	0.002629	-0.03864	0.002628967	0.038644508
15.1346	0.5345	0.536229	8.089444	8.115619	0.001729	-0.02618	0.001729489	0.026175118
15.5311	0.4275	0.42955	6.639545	6.671392	0.00205	-0.03185	0.002050494	0.03184643
15.8929	0.3185	0.318831	5.061889	5.067154	0.000331	-0.00527	0.000331286	0.005265092
16.2229	0.2085	0.207454	3.382475	3.365513	-0.00105	0.016962	0.001045564	0.016962087
16.5241	0.101	0.096231	1.668934	1.59013	-0.00477	0.078804	0.004769012	0.078803628
16.7987	-0.008	-0.00828	-0.13439	-0.13911	-0.00028	0.004717	0.000280774	0.004716631
17.0499	-0.111	-0.11092	-1.89254	-1.89116	8.08E-05	-0.00138	8.07728E-05	0.001377168
17.2793	-0.209	-0.20927	-3.61137	-3.61599	-0.00027	0.004614	0.000267051	0.004614456
17.4885	-0.303	-0.30093	-5.29902	-5.26284	0.002068	-0.03617	0.002068465	0.036174351

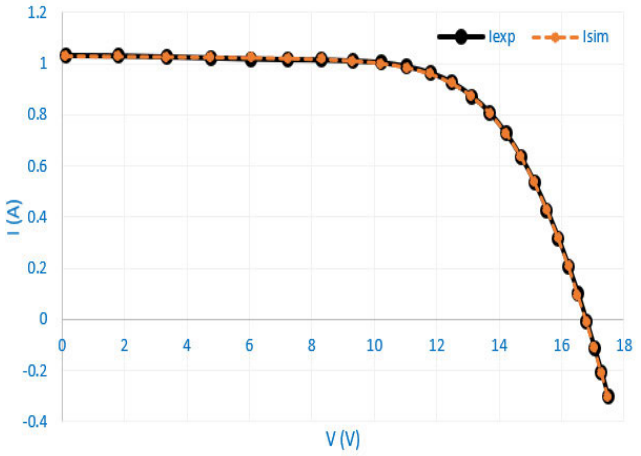

FIGURE 13. I-V curve of experimental and simulated current of FBIA on PVDDM of PWP 201 polycrystalline.

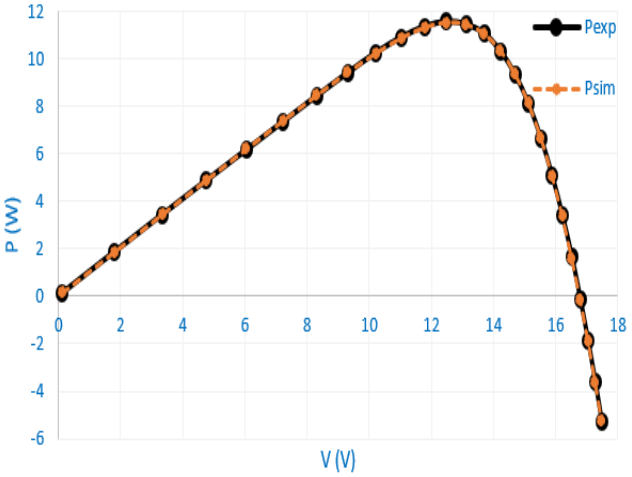

FIGURE 14. P-V curve of experimental and simulated current of FBIA on PVDDM of PWP 201 polycrystalline.

TABLE 9. The Min, Mean, Max and Std of both recent and reported optmization techniques on PVTDM of PWP 201 polycrystalline Module.

	min	mean	max	Std
EO	0.002425	0.002436	0.002477	1.11E-05
HEAP	0.002437	0.002495	0.002586	3.01E-05
JFS	0.002426	0.002432	0.002443	5.04E-06
MPA	0.002469	0.00263	0.003679	0.20E-4
MRFO	0.002428	0.002445	0.002527	2.3E-05
FBIA	0.002426	0.002437	0.00246	1.06E-05

TABLE 10. Parameter estimation extracted from of both recent and reported optmization techniques on PVTDM of PWP 201 polycrystalline Module.

	EO	HEAP	JFS	MPA	MRFO	FBIA
Iph	1.03045	1.03101	1.03051	1.02948	1.03071	1.03054
Rs	0.03335	0.03322	0.03336	0.03301	0.03346	0.03334
Rsh	27.5718	26.1645	27.4191	33.7098	26.3606	27.4415
Io1	7.6E-07	0	1.1E-06	5.3E-07	5.6E-07	4.2E-07
n1	1.36248	1.0555	1.36142	1.29883	1.37781	1.35364
Io2	1.6E-07	0	1.2E-06	3.7E-06	9.4E-07	2.8E-07
n2	1.33951	1.35275	1.34545	1.38889	1.33965	1.36779
Io3	2.6E-06	3.6E-06	1.2E-06	6.6E-11	1.9E-06	2.8E-06
n3	1.35022	1.35488	1.34916	1.38626	1.34584	1.3507

3) CASE3: PVTDM

FBIA is employed on PVTDM for the first time, in this case, where the optimal solution is compared with respect to those manifested by various reported and recently developed optimization techniques as in Table 9. It is apparently seen that the FBIA finds a minimum standard deviation of 1.06E-05,

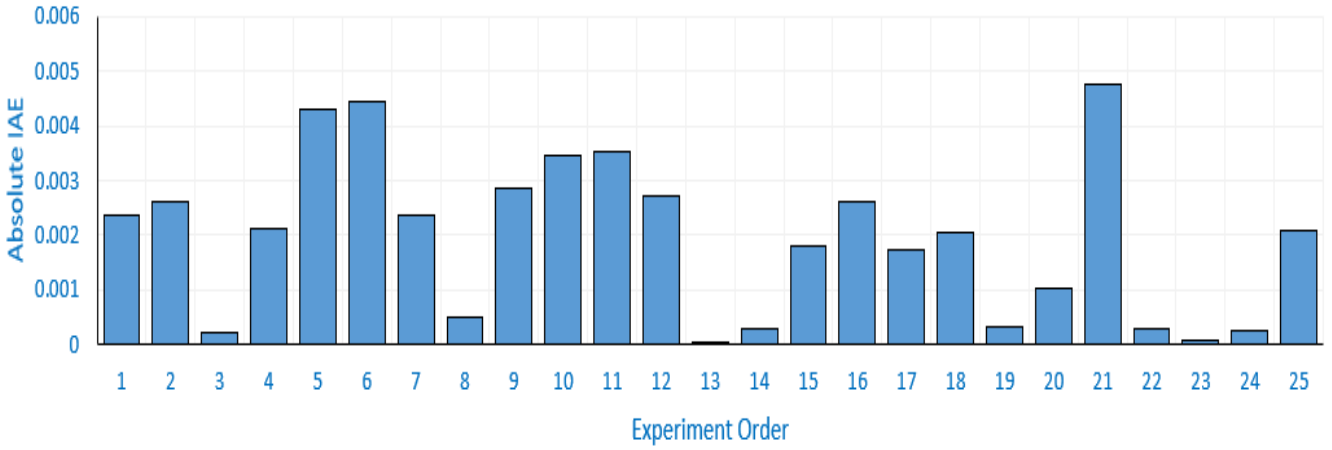

FIGURE 15. The absolute error of experimental and simulated current of FBIA on PVDDM of PWP 201 polycrystalline.

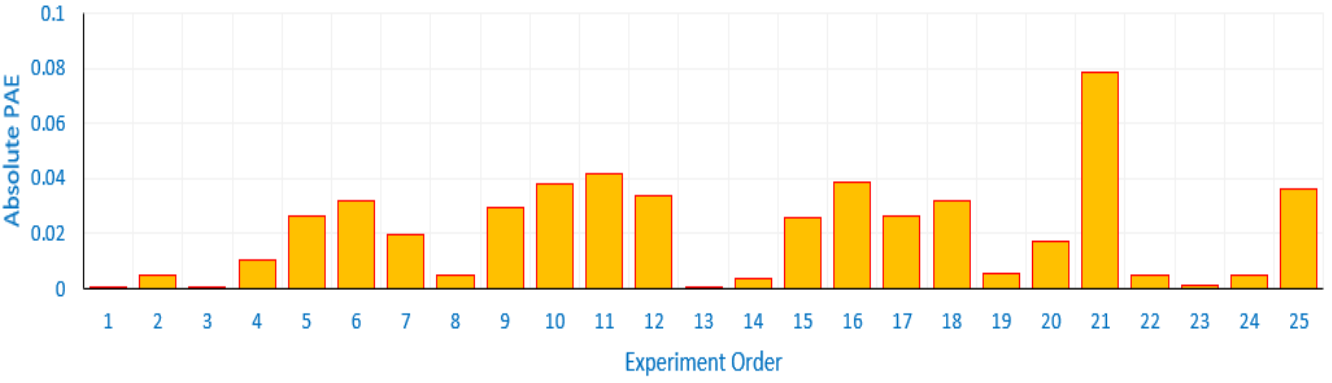

FIGURE 16. The absolute error of experimental and simulated power of FBIA on PVDDM of PWP 201 polycrystalline.

which is less than EO, HEAP, JFS, MPA, and MRFO, where they acquired standard deviation of 1.11E-05, 3.01E-05, 5.04E-06, 0.20E-04, 1.36E-05, and 2.3E-05, respectively. Table 10 describes the parameter estimation extracted from both recent and reported optimization techniques on PVTDM of PWP 201 polycrystalline module, where the proposed FBIA achieves the most accurate results for these parameters with respect to other techniques

Fig. 17 illustrates the RMSE of FBIA compared to recent optmization techniques, which are JFS, MRFO, HEAP, EO, MPA on PVDDM of PWP 201 polycrystalline Module. The RMSE data were obtained depending on 30 Runs for all recent algorithms. The proposed FBIA achives the lowest RMSE value among the recently developed techniques in the literature. The RMSE value of FBIA accounts for 0.002425. For this case, the convergence characteristics of the FBIA are stable and the arrival of the optimal solution is faster than the other recent optmization techniques in Fig. 18. Figs. 19 and 20 provide the simulated behavior of the PVTDM result compared with respect to the data that used for the parameter estimation. These figures show he current–voltage (I-V) and the power-voltage (P-V) curves of the PVTDM. Table 11 demonstrates the points of experimental, simulated current values, and the absolute errors between them. Moreover, it manifests the experimental, simulated power values, and the absolute errors between them when employing the FBIA on PVSDM of PWP 201 polycrystalline. In addition, Figs. 21 and 22 give the absolute errors of experimental and simulated currents for FBIA on PVSDM of PWP 201 polycrystalline module for 25 runs according to the standard benchmark module.

B. KYOCERA KC200GT PV MODULE

The second test system, which is Kyocera KC200GT PV Module, 57 mm diameter silicon solar cell, were tested to get the measured data with variation of both irradiance and temperature. In this section, FBIA is employed on the Kyocera KC200GT module to show the I-V characteristics of the KC200GT module experimented and simulated by the three-model system, which are PVSDM, PVDDM and PVTDM as illustrated below.

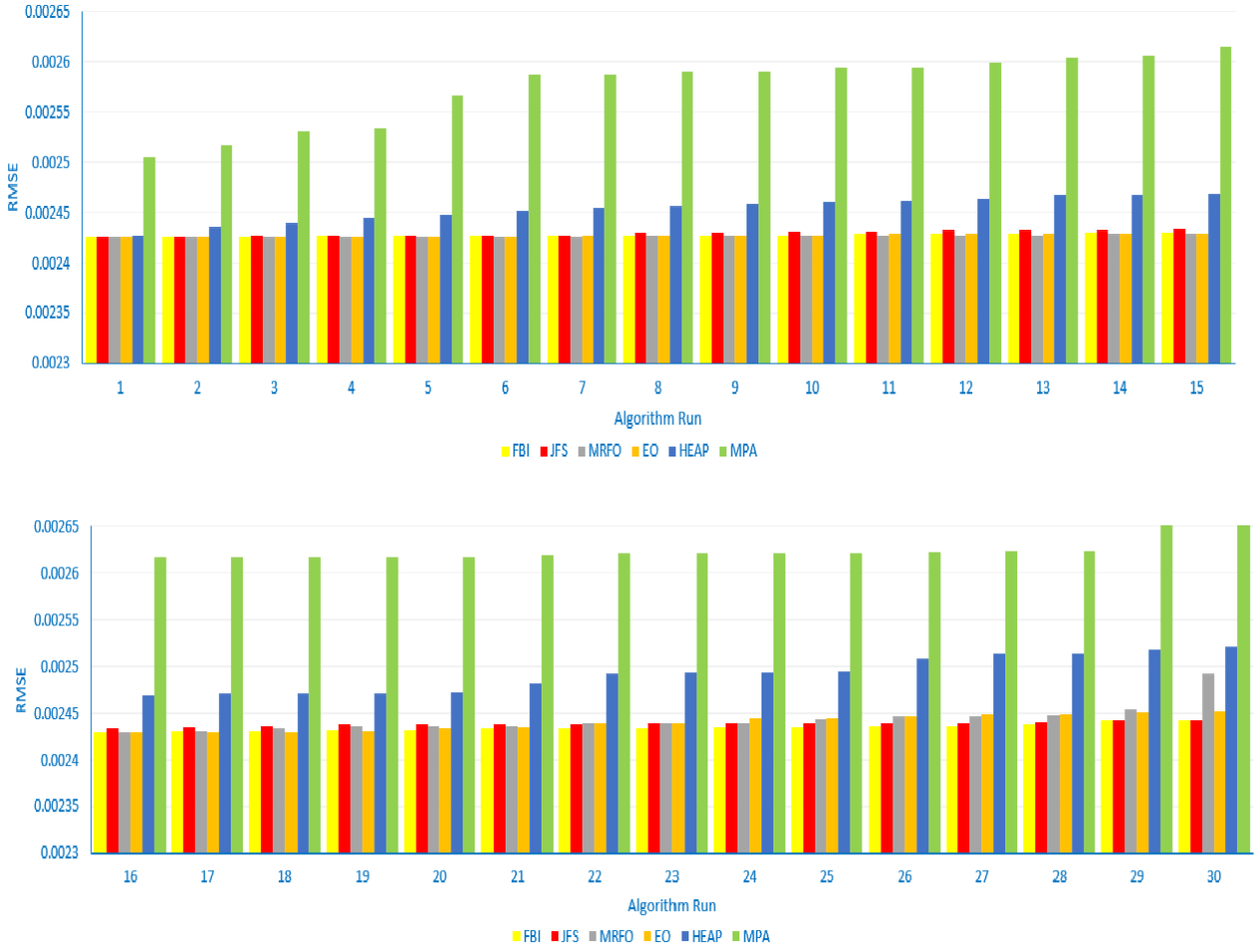

FIGURE 17. RMSE of FBIA compared to recent optmization techniques on PVTDM of PWP 201 polycrystalline Module.

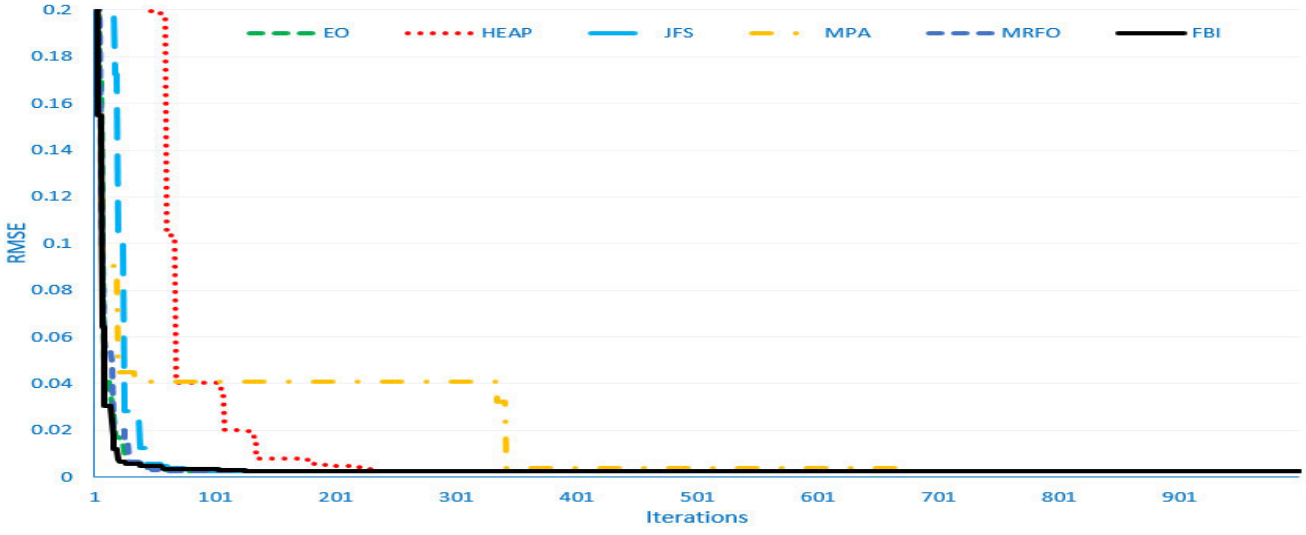

FIGURE 18. Convergence charactrictics of FBIA versus other recent optmization techniques on PVTDM of PWP 201 polycrystalline.

TABLE 11. Experimental and simulated current and power of FBIA on PVTDM of PWP 201 polycrystalline and the absolute errors among them.

.Vexp	Iexp	Isim	Pexp	Psim	IAE	PAE	Absolut IAE	Absolut PAE
0.1248	1.0315	1.029151	0.128731	0.1284	-0.0023	0.0003	0.0023	0.0003
1.8093	1.03	1.027423	1.863579	1.8589	-0.0026	0.0047	0.0026	0.0047
3.3511	1.026	1.025793	3.438229	3.4375	-0.0002	0.0007	0.0002	0.0007
4.7622	1.022	1.024165	4.866968	4.8773	0.0022	-0.0103	0.0022	0.0103
6.0538	1.018	1.022355	6.162768	6.1891	0.0044	-0.0264	0.0044	0.0264
7.2364	1.0155	1.019997	7.348564	7.3811	0.0045	-0.0325	0.0045	0.0325
8.3189	1.014	1.016428	8.435365	8.4556	0.0024	-0.0202	0.0024	0.0202
9.3097	1.01	1.010554	9.402797	9.408	0.0006	-0.0052	0.0006	0.0052
10.2163	1.0035	1.000673	10.25206	10.2232	-0.0028	0.0289	0.0028	0.0289
11.0449	0.988	0.984573	10.91236	10.8745	-0.0034	0.0378	0.0034	0.0378
11.8018	0.963	0.959522	11.36513	11.3241	-0.0035	0.041	0.0035	0.041
12.4929	0.9255	0.922813	11.56218	11.5286	-0.0027	0.0336	0.0027	0.0336
13.1231	0.8725	0.87255	11.4499	11.4506	0.0001	-0.0007	0.0001	0.0007
13.6983	0.8075	0.807208	11.06138	11.0574	-0.0003	0.004	0.0003	0.004
14.2221	0.7265	0.728261	10.33236	10.3574	0.0018	-0.025	0.0018	0.025
14.6995	0.6345	0.637062	9.326833	9.3645	0.0026	-0.0377	0.0026	0.0377
15.1346	0.5345	0.536144	8.089444	8.1143	0.0016	-0.0249	0.0016	0.0249
15.5311	0.4275	0.429452	6.639545	6.6699	0.002	-0.0303	0.002	0.0303
15.8929	0.3185	0.318726	5.061889	5.0655	0.0002	-0.0036	0.0002	0.0036
16.2229	0.2085	0.207348	3.382475	3.3638	-0.0012	0.0187	0.0012	0.0187
16.5241	0.101	0.096131	1.668934	1.5885	-0.0049	0.0805	0.0049	0.0805
16.7987	-0.008	-0.00837	-0.13439	-0.1406	-0.0004	0.0062	0.0004	0.0062
17.0499	-0.111	-0.11099	-1.89254	-1.8923	0	-0.0002	0	0.0002
17.2793	-0.209	-0.20931	-3.61137	-3.6168	-0.0003	0.0054	0.0003	0.0054
17.4885	-0.303	-0.30095	-5.29902	-5.2632	0.002	-0.0358	0.002	0.0358

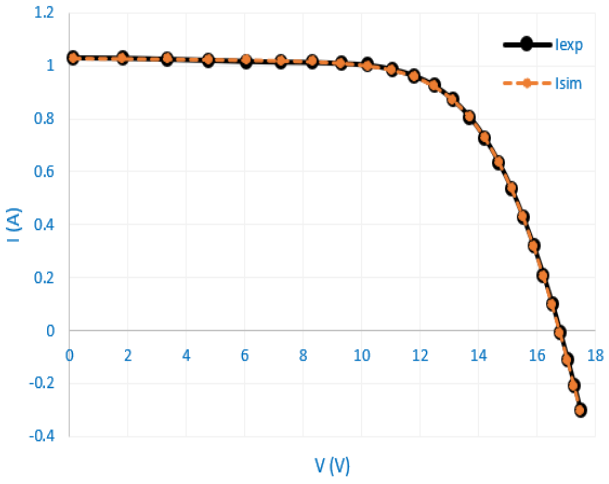

FIGURE 19. I-V curve of experimental and simulated current of FBIA on PVTDM of PWP 201 polycrystalline.

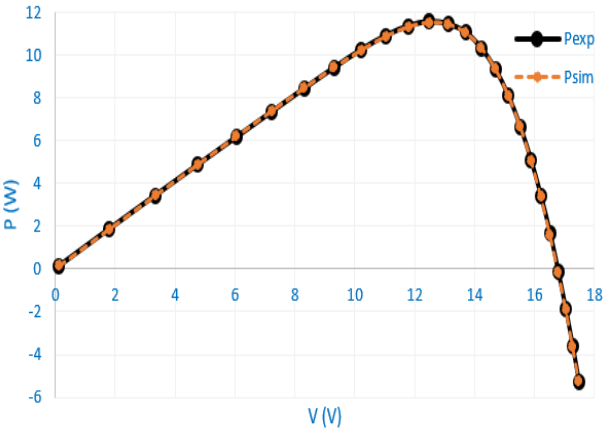

FIGURE 20. P-V curve of experimental and simulated current of FBIA on PVTDM of PWP 201 polycrystalline.

1) CASE 1: PVSDM

This part explains the I-V and P-V characteristics of the KC200GT module that are experimented and simulated when using PVSDM with variation of both irradiance and temperature. FBIA is implemented on this type to simulate 15 points with different values of current and voltage. There are variations in the values of currents and voltage when varying the values of irradiance and temperature as depicted in Figs. 23 and 24.

Fig. 23 manifests I-V curve of the KC200GT module experimented and simulated by the PVSDM for irradiance of 1000 W/m^2 and varied temperature, where the voltage values of the three curves under different temperature values are decreased when the values of temperature increases. On the other hand, the values of currents are dramatically increased when rising the irradiance values, while the temperature value is constant at 25 °C as illustrated in Fig. 24.

Similarly, the P-V characteristics of the KC200GT module are experimented and simulated when using PVSDM with variation of both irradiance and temperature as described in Figs. 25 and 26 where the irradiance has changed from 200, 400, 600, 800, and 1000 W/m^2 and the temperature accounts for 25, 47, 50, and 75°C. These variations in the temperature

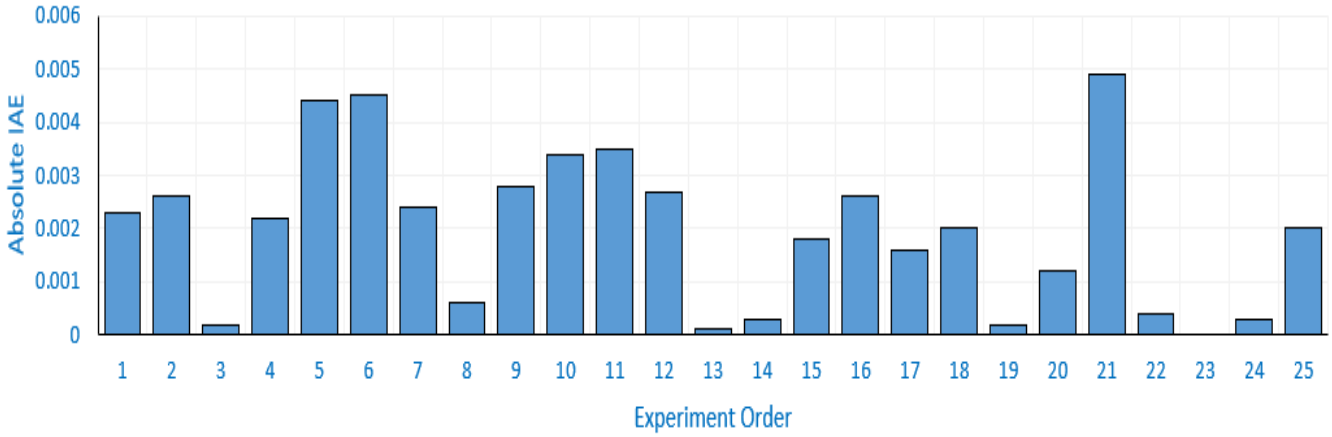

FIGURE 21. The absolute error of experimental and simulated current of FBIA on PVTDM of PWP 201 polycrystalline.

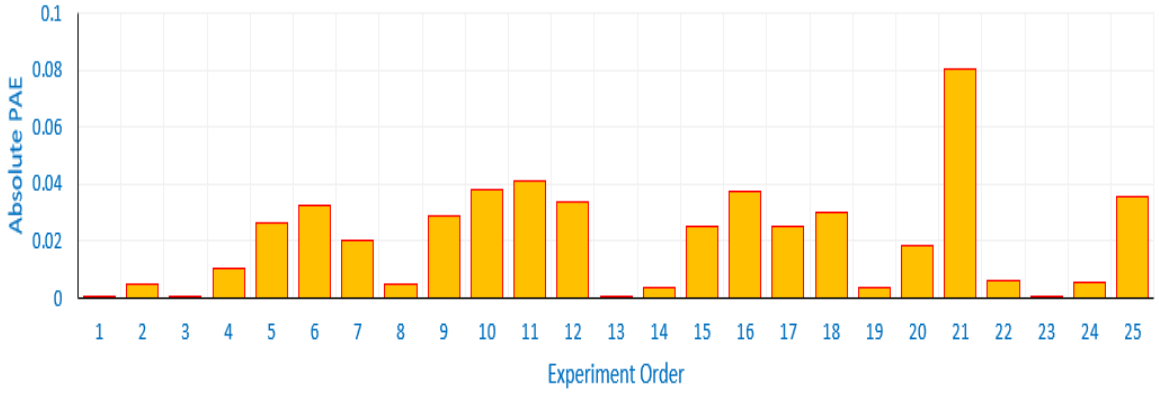

FIGURE 22. The absolute error of experimental and simulated power of FBIA on PVTDM of PWP 201 polycrystalline.

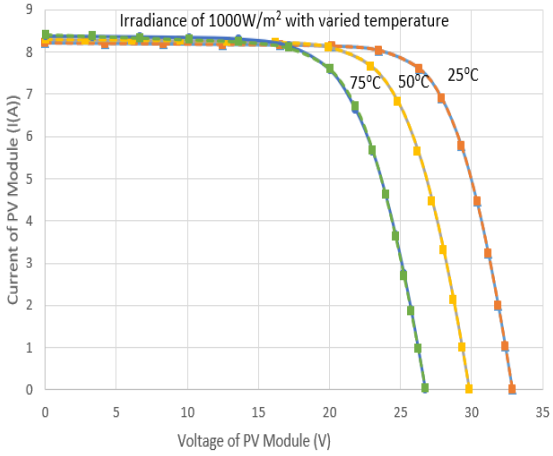

FIGURE 23. I-V characteristics of the KC200GT module experimented and simulated by the PVSDM for irradiance of 1000W/m^2 and varied temperature.

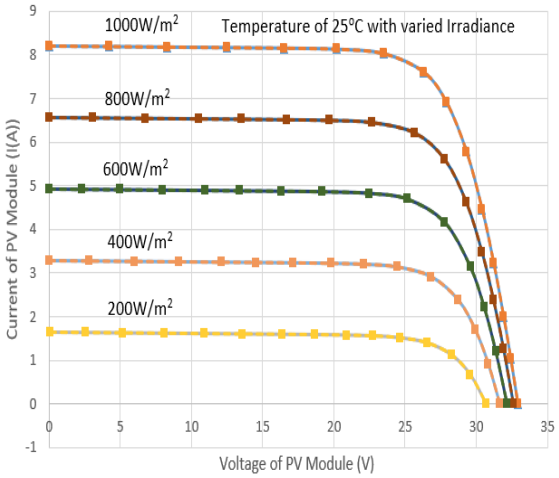

FIGURE 24. I-V characteristics of the KC200GT module experimented and simulated by the PVSDM for temperature of 25 °C.

and irradiance values can change the values of power of the model versus the voltage. Fig. 25 manifests P-V curve of that module experimented and simulated by the PVSDM for irradiance of 1000 W/m^2 and varied temperature, where the voltage values of the three curves under different temperature values decreased when the temperature increased from 25,

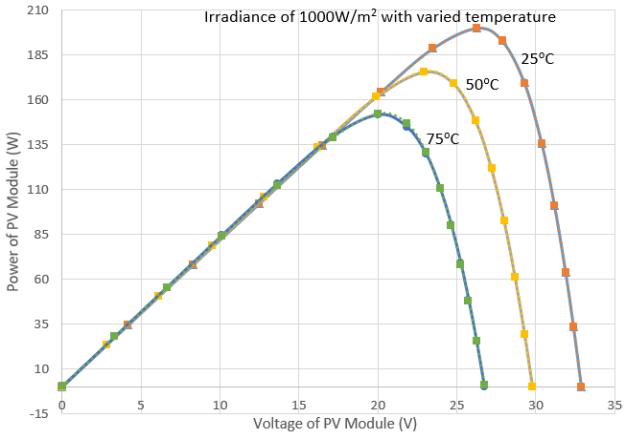

FIGURE 25. P-V characteristics of the KC200GT module experimented and simulated by the PVSDM for irradiance of 1000W/m^2 and varied temperature.

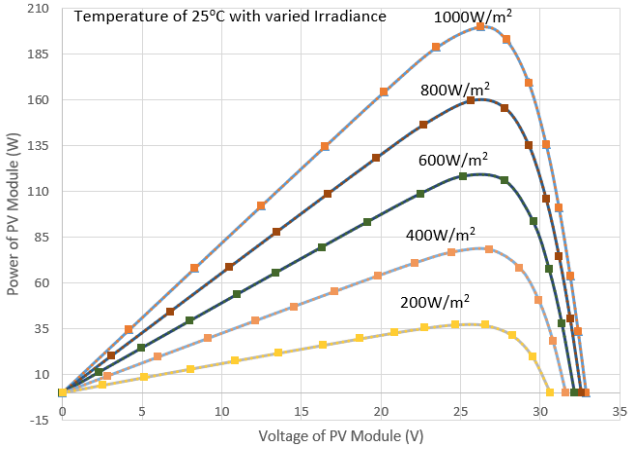

FIGURE 26. P-V characteristics of the KC200GT module experimented and simulated by the PVSDM with fixed temperature of 25 °C and varied irradiance.

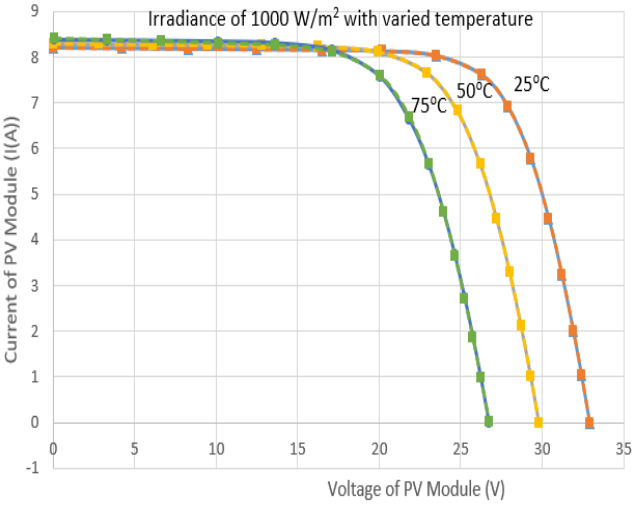

FIGURE 27. I-V characteristics of the KC200GT module experimented and simulated by the PVDDM with irradiance of 1000W/m^2.

50, and 75°C, respectively. However, the values of power are sharply increased when rising the irradiance values, while the temperature value is constant at 25 °C as in Fig. 26.

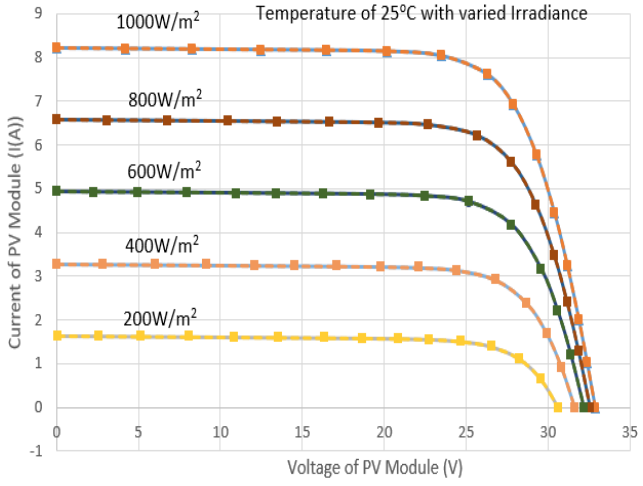

FIGURE 28. I-V characteristics of the KC200GT module experimented and simulated by the PVDDM for temperature of 25 °C.

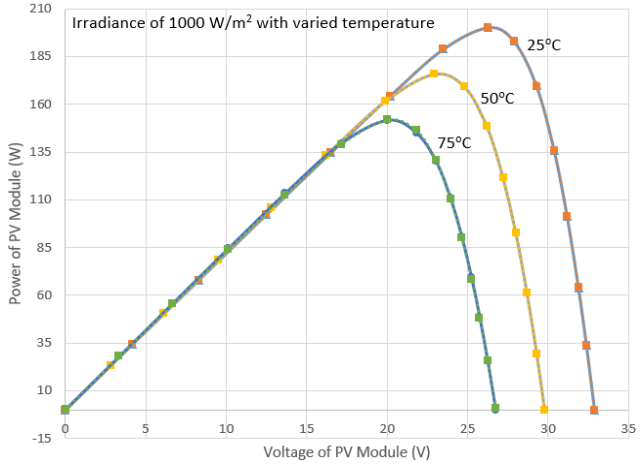

FIGURE 29. P-V characteristics of the KC200GT module experimented and simulated by the PVDDM for irradiance of 1000W/m^2.

2) CASE 2: PVDDM

This part introduces the I-V and P-V characteristics of the KC200GT module that are experimented and simulated with variation of both irradiance and temperature when using PVDDM. In this case, FBIA is employed on this type to simulate 15 points with different values of current and voltage. It is apparently clear that there are variations in the values of currents and voltage when varying the values of irradiance and temperature as depicted in Figs. 27 and 28. Fig. 27 manifests I-V curve of the above mentioned module experimented and simulated by the PVDDM for irradiance of 1000 W/m^2 and varied temperature, where the voltage values of the three curves under different temperature values are decreased when the values of temperature increases. On the other hand, the values of currents dramatically increased when rising the irradiance values, while the temperature value is constant at 25°C as in Fig. 28.

Equally, the P-V characteristics of the KC200GT module are experimented and simulated when using PVDDM with variation of temperature and irradiance as reflected in

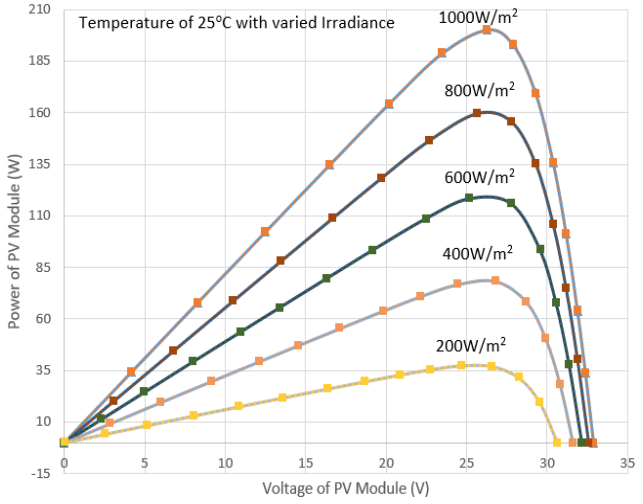

FIGURE 30. P-V characteristics of the KC200GT module experimented and simulated by the PVDDM at 25 °C and varied irradiance.

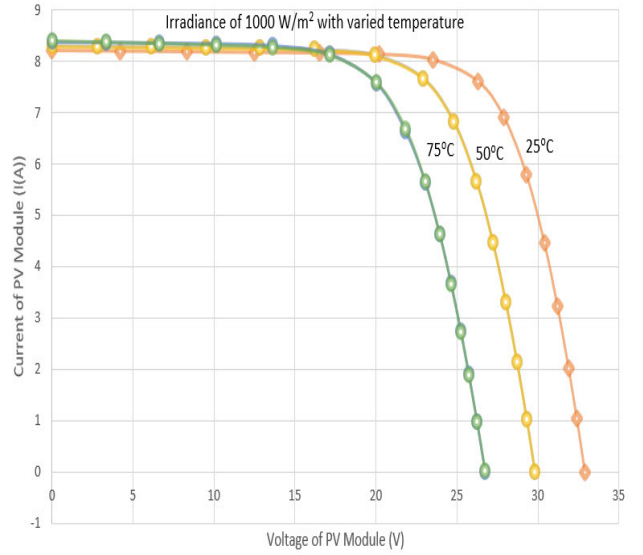

FIGURE 31. I-V characteristics of the KC200GT module experimented and simulated by the PVTDM for irradiance of 1000W/m^2.

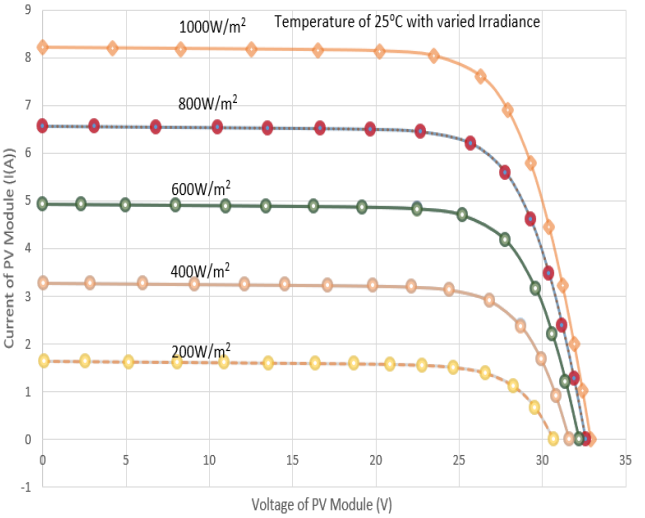

FIGURE 32. I-V characteristics of the KC200GT module experimented and simulated by the PVTDM for temperature of 25 °C.

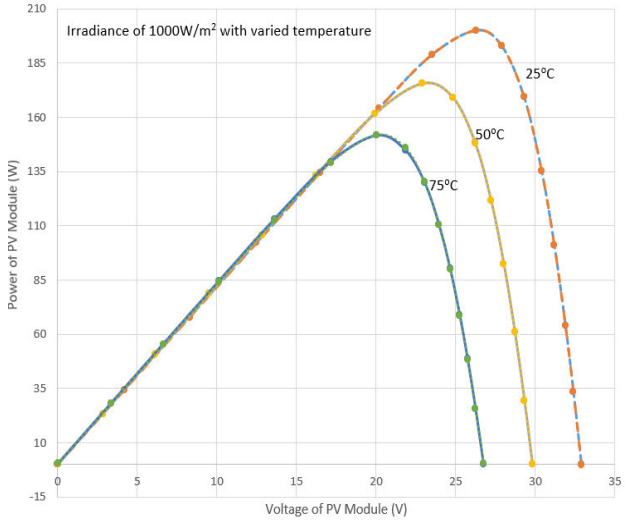

FIGURE 33. P-V characteristics of the KC200GT module experimented and simulated by the PVTDM for irradiance of 1000W/m^2.

Figs. 29 and 30, where the irradiance has changed from 200, 400, 600, 800, and 1000 W/m^2 and the temperature accounts for 25, 47, 50, and 75°C. These variations in the temperature and irradiance values can change the values of power of the model versus the voltage. Fig. 29 displays the P-V curve of that module experimented and simulated by the PVDDM for irradiance of 1000 W/m^2 and varied temperature, where the voltage values of the three curves under different temperature values decreased when the temperature increased from 25, 50, and 75°C, respectively, whereas the values of power is sharply increased when rising the irradiance values, while the temperature value is constant at 25 °C as in Fig. 30.

3) CASE 3: PVTDM

This case elaborates the I-V and P-V characteristics of the KC200GT module that are experimented and simulated when using PVTDM with variation of both irradiance and temperature. The proposed FBIA is applied on this type to simulate 15 points with various values of current and voltage. There are variations in the values of currents and voltage when varying the values of irradiance and temperature as characterized in Figs. 31 and 32. Fig. 31 manifests I-V curve of the KC200GT module experimented and simulated by the PVTDM for irradiance of 1000 W/m^2 and varied temperature, where the voltage values of the three curves under different temperature values decreased when the values of temperature increased. On the other hand, the values of currents dramatically increased when rising the irradiance values, while the temperature value is constant at 25 °C as illustrated in Fig. 32. Similarly, the P-V characteristics of the KC200GT module are experimented and simulated when using PVTDM with variation of both irradiance and temperature as described in Figs. 33 and 34 where the irradiance has changed from 200,

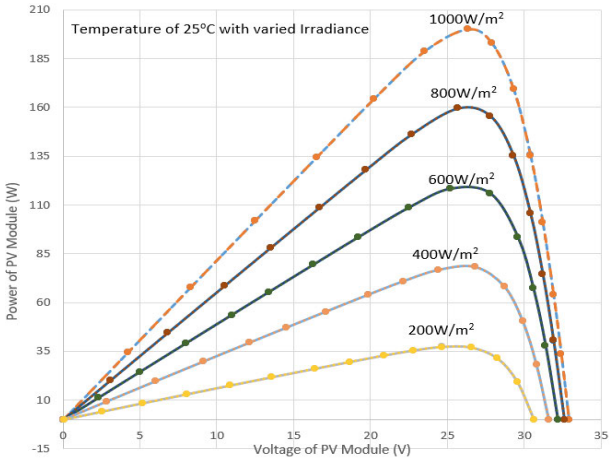

FIGURE 34. P-V characteristics of the KC200GT module experimented and simulated by the PVTDM at 25 °C and varied irradiance.

TABLE 12. Parameter estimation extracted from FBIA on PVSDM, PVDDM, and PVTDM of KC-200GT Module.

Parameters	PVSDM	PVDDM	PVTDM
Iph	8.216339	8.214985	8.215585
Rs	0.004829	0.004813	0.00483
Rsh	6.323365	6.566162	6.502457
Io1	2.61E-08	2.75E-08	2.41E-08
n1	1.212565	1.215784	1.20815
Io2	-	2.4E-08	6.13E-08
n2	-	1.95351	1.936446
Io3	-	-	3.2E-07
n3	-	-	1.993933
RMSE	0.000734	0.000962	0.000721
SSE	8.08E-06	1.39E-05	7.81E-06

400, 600, 800, and 1000 W/m^2 and the temperature accounts for 25, 47, 50, and 75°C. These variations in the temperature and irradiance values can change the values of power of the model versus the voltage. Fig. 33 manifests P-V curve of that module experimented and simulated by the PVTDM for irradiance of 1000 W/m^2 and varied temperature, where the voltage values of the three curves under different temperature values decreased when the temperature increased from 25, 50, and 75°C, respectively. However, the values of power are sharply increased when rising the irradiance values, while the temperature value is constant at 25 °C as in Fig. 34.

Table 12 shows the standard deviation and the RMSE errors of the module KC-200GT characteristics attained by PVTDM are 7.81E-06, and 0.000721, respectively, that are less than the obtained by PVSDM as 8.08E-06, 0.000734, and by PVDDM, as 1.39E-05, 0.000962, respectively.

V. CONCLUSION

FBIA is a new meta-heuristic optimization technique and implemented on the PV parameter extraction problem. This article has presented a novel application of the FBIA approach to properly extract the five, seven, and nine parameters of PVMSD, PVMDD, and PVMTD of both Photowatt-PWP 201 polycrystalline and Kyocera KC200GT PV modules. The delivered solutions for the PVMSD, PVMDD, and PVMTD of both Photowatt-PWP 201 polycrystalline and Kyocera KC200GT modules test system are compared with respect to the recent optimization techniques that have developed in this article and the reported ones in literatures. The three models are inspected to depict the superiority of the FBIA. The proposed FBIA algorithm is successfully implemented to design optimally the parameters of two Photowatt-PWP 201 polycrystalline and Kyocera KC200GT modules. The optimal parameters using the FBIA model are coherent compared to the other diverse algorithms. The FBIA approach has recorded less optimal fitness values for Photowatt-PWP 201 and Kyocera KC200GT modules.

ACKNOWLEDGMENT

The authors would like to acknowledge the financial support received from Taif University Researchers Supporting Project Number (TURSP-2020/34), Taif University, Taif, Saudi Arabia.

REFERENCES

[1] M. H. Qais, H. M. Hasanien, and S. Alghuwainem, "Parameters extraction of three-diode photovoltaic model using computation and Harris Hawks optimization," *Energy*, vol. 195, Mar. 2020, Art. no. 117040.

[2] M. H. Qais, H. M. Hasanien, and S. Alghuwainem, "Transient search optimization for electrical parameters estimation of photovoltaic module based on datasheet values," *Energy Convers. Manage.*, vol. 214, Jun. 2020, Art. no. 112904.

[3] D. Yousri, D. Allam, M. B. Eteiba, and P. N. Suganthan, "Static and dynamic photovoltaic models' parameters identification using chaotic heterogeneous comprehensive learning particle swarm optimizer variants," *Energy Convers. Manage.*, vol. 182, pp. 546–563, Feb. 2019.

[4] D. Yousri, S. B. Thanikanti, D. Allam, V. K. Ramachandaramurthy, and M. B. Eteiba, "Fractional chaotic ensemble particle swarm optimizer for identifying the single, double, and three diode photovoltaic models' parameters," *Energy*, vol. 195, Mar. 2020, Art. no. 116979.

[5] D. S. H. Chan, J. R. Phillips, and J. C. H. Phang, "A comparative study of extraction methods for solar cell model parameters," *Solid-State Electron.*, vol. 29, no. 3, pp. 329–337, Mar. 1986.

[6] A. Jain, "Exact analytical solutions of the parameters of real solar cells using lambert W-function," *Sol. Energy Mater. Sol. Cells*, vol. 81, no. 2, pp. 269–277, Feb. 2004.

[7] H. Saleem and S. Karmalkar, "An analytical method to extract the physical parameters of a solar cell from four points on the illuminated $J-V$ curve," *IEEE Electron Device Lett.*, vol. 30, no. 4, pp. 349–352, Apr. 2009.

[8] E. I. Batzelis and S. A. Papathanassiou, "A method for the analytical extraction of the single-diode PV model parameters," *IEEE Trans. Sustain. Energy*, vol. 7, no. 2, pp. 504–512, Apr. 2016.

[9] A. H. Soeriyadi, L. Wang, B. Conrad, D. Li, A. Lochtefeld, A. Gerger, A. Barnett, and I. Perez-Wurfl, "Extraction of essential solar cell parameters of subcells in a tandem structure with a novel three-terminal measurement technique," *IEEE J. Photovolt.*, vol. 8, no. 1, pp. 327–332, Jan. 2018.

[10] B. Romero, G. del Pozo, B. Arredondo, D. Martín-Martín, M. P. Ruiz Gordoa, A. Pickering, A. Pérez-Rodríguez, E. Barrena, and F. J. García-Sánchez, "S-shaped $I-V$ characteristics of organic solar cells: Solving Mazhari's lumped-parameter equivalent circuit model," *IEEE Trans. Electron Devices*, vol. 64, no. 11, pp. 4622–4627, Nov. 2017.

[11] M. R. AlRashidi, M. F. AlHajri, K. M. El-Naggar, and A. K. Al-Othman, "A new estimation approach for determining the I–V characteristics of solar cells," *Sol. Energy*, vol. 85, no. 7, pp. 1543–1550, Jul. 2011.

[12] H. Wei, J. Cong, X. Lingyun, and S. Deyun, "Extracting solar cell model parameters based on chaos particle swarm algorithm," in *Proc. Int. Conf. Electr. Inf. Control Eng.*, Apr. 2011, pp. 398–402.

[13] X. Ma, W.-H. Huang, E. Schnabel, M. Kohl, J. Brynjarsdottir, J. L. Braid, and R. H. French, "Data-driven I-V feature extraction for photovoltaic modules," *IEEE J. Photovolt.*, vol. 9, no. 5, pp. 1405–1412, Sep. 2019.

[14] P. Lin, S. Cheng, W. Yeh, Z. Chen, and L. Wu, "Parameters extraction of solar cell models using a modified simplified swarm optimization algorithm," *Sol. Energy*, vol. 144, pp. 594–603, Mar. 2017.

[15] I. A. Ibrahim, M. J. Hossain, B. C. Duck, and C. J. Fell, "An adaptive wind-driven optimization algorithm for extracting the parameters of a single-diode PV cell model," *IEEE Trans. Sustain. Energy*, vol. 11, no. 2, pp. 1054–1066, Apr. 2020.

[16] H. K. Mehta, H. Warke, K. Kukadiya, and A. K. Panchal, "Accurate expressions for single-diode-model solar cell parameterization," *IEEE J. Photovolt.*, vol. 9, no. 3, pp. 803–810, May 2019.

[17] A. A. Cardenas, M. Carrasco, F. Mancilla-David, A. Street, and R. Cardenas, "Experimental parameter extraction in the single-diode photovoltaic model via a reduced-space search," *IEEE Trans. Ind. Electron.*, vol. 64, no. 2, pp. 1468–1476, Feb. 2017.

[18] A. K. Panchal, "I–V data operated high-quality photovoltaic solution through per-unit single-diode model," *IEEE J. Photovolt.*, vol. 10, no. 4, pp. 1175–1184, Jul. 2020.

[19] F. J. Toledo, J. M. Blanes, and V. Galiano, "Two-step linear least-squares method for photovoltaic single-diode model parameters extraction," *IEEE Trans. Ind. Electron.*, vol. 65, no. 8, pp. 6301–6308, Aug. 2018.

[20] V. J. Chin and Z. Salam, "Coyote optimization algorithm for the parameter extraction of photovoltaic cells," *Sol. Energy*, vol. 194, pp. 656–670, Dec. 2019.

[21] H. M. Waly, H. Z. Azazi, D. S. M. Osheba, and A. E. El-Sabbe, "Parameters extraction of photovoltaic sources based on experimental data," *IET Renew. Power Gener.*, vol. 13, no. 9, pp. 1466–1473, Jul. 2019.

[22] S. Gude and K. C. Jana, "Parameter extraction of photovoltaic cell using an improved cuckoo search optimization," *Sol. Energy*, vol. 204, pp. 280–293, Jul. 2020.

[23] B. Subudhi and R. Pradhan, "Bacterial foraging optimization approach to parameter extraction of a photovoltaic module," *IEEE Trans. Sustain. Energy*, vol. 9, no. 1, pp. 381–389, Jan. 2018.

[24] Z. Liao, Z. Chen, and S. Li, "Parameters extraction of photovoltaic models using triple-phase teaching-learning-based optimization," *IEEE Access*, vol. 8, pp. 69937–69952, 2020.

[25] A. A. Z. Diab, H. M. Sultan, T. D. Do, O. M. Kamel, and M. A. Mossa, "Coyote optimization algorithm for parameters estimation of various models of solar cells and PV modules," *IEEE Access*, vol. 8, pp. 111102–111140, 2020.

[26] R. Chenouard and R. A. El-Sehiemy, "An interval branch and bound global optimization algorithm for parameter estimation of three photovoltaic models," *Energy Convers. Manage.*, vol. 205, Feb. 2020, Art. no. 112400.

[27] A. A. Z. Diab, H. M. Sultan, R. Aljendy, A. S. Al-Sumaiti, M. Shoyama, and Z. M. Ali, "Tree growth based optimization algorithm for parameter extraction of different models of photovoltaic cells and modules," *IEEE Access*, vol. 8, pp. 119668–119687, 2020.

[28] R. C. M. Gomes, M. A. Vitorino, M. B. de Rossiter Correa, D. A. Fernandes, and R. Wang, "Shuffled complex evolution on photovoltaic parameter extraction: A comparative analysis," *IEEE Trans. Sustain. Energy*, vol. 8, no. 2, pp. 805–815, Apr. 2017.

[29] M. A. Soliman, H. M. Hasanien, and A. Alkuhayli, "Marine predators algorithm for parameters identification of triple-diode photovoltaic models," *IEEE Access*, vol. 8, pp. 155832–155842, 2020.

[30] M. A. El-Hameed, M. M. Elkholy, and A. A. El-Fergany, "Three-diode model for characterization of industrial solar generating units using manta-rays foraging optimizer: Analysis and validations," *Energy Convers. Manage.*, vol. 219, Sep. 2020, Art. no. 113048.

[31] A. M. Humada, M. Hojabri, S. Mekhilef, and H. M. Hamada, "Solar cell parameters extraction based on single and double-diode models: A review," *Renew. Sustain. Energy Rev.*, vol. 56, pp. 494–509, Apr. 2016.

[32] K. Ishaque, Z. Salam, S. Mekhilef, and A. Shamsudin, "Parameter extraction of solar photovoltaic modules using penalty-based differential evolution," *Appl. Energy*, vol. 99, pp. 297–308, Nov. 2012.

[33] J.-S. Chou and N.-M. Nguyen, "FBI inspired meta-optimization," *Appl. Soft Comput.*, vol. 93, Aug. 2020, Art. no. 106339.

[34] T. Easwarakhanthan, J. Bottin, I. Bouhouch, and C. Boutrit, "Nonlinear minimization algorithm for determining the solar cell parameters with microcomputers," *Int. J. Sol. Energy*, vol. 4, no. 1, pp. 1–12, Jan. 1986.

[35] A. Askarzadeh and A. Rezazadeh, "Artificial bee swarm optimization algorithm for parameters identification of solar cell models," *Appl. Energy*, vol. 102, pp. 943–949, Feb. 2013.

[36] X. Gao, Y. Cui, J. Hu, G. Xu, Z. Wang, J. Qu, and H. Wang, "Parameter extraction of solar cell models using improved shuffled complex evolution algorithm," *Energy Convers. Manage.*, vol. 157, pp. 460–479, Feb. 2018.

[37] L. Guo, Z. Meng, Y. Sun, and L. Wang, "Parameter identification and sensitivity analysis of solar cell models with cat swarm optimization algorithm," *Energy Convers. Manage.*, vol. 108, pp. 520–528, Jan. 2016.

[38] J.-S. Chou and D.-N. Truong, "A novel Metaheuristic optimizer inspired by behavior of jellyfish in ocean," *Appl. Math. Comput.*, vol. 389, Jan. 2021, Art. no. 125535.

[39] A. M. Shaheen, A. R. Ginidi, R. A. El-Sehiemy, and S. S. M. Ghoneim, "Economic power and heat dispatch in cogeneration energy systems using manta ray foraging optimizer," *IEEE Access*, vol. 8, pp. 208281–208295, 2020, doi: 10.1109/access.2020.3038740.

[40] E. E. Elattar, A. M. Shaheen, A. M. Elsayed, and R. A. El-Sehiemy, "Optimal power flow with emerged technologies of voltage source converter stations in meshed power systems," *IEEE Access*, vol. 8, pp. 166963–166979, 2020, doi: 10.1109/access.2020.3022919.

[41] A. Faramarzi, M. Heidarinejad, S. Mirjalili, and A. H. Gandomi, "Marine predators algorithm: A nature-inspired Metaheuristic," *Expert Syst. Appl.*, vol. 152, Aug. 2020, Art. no. 113377.

[42] A. M. Shaheen, A. M. Elsayed, R. A. El-Sehiemy, and A. Y. Abdelaziz, "Equilibrium optimization algorithm for network reconfiguration and distributed generation allocation in power systems," *Appl. Soft Comput.*, vol. 98, Jan. 2021, Art. no. 106867, doi: 10.1016/j.asoc.2020.106867.

[43] D. T. Abdul-hamied, A. M. Shaheen, W. A. Salem, W. I. Gabr, and R. A. El-sehiemy, "Equilibrium optimizer based multi dimensions operation of hybrid AC/DC grids," *Alexandria Eng. J.*, to be published, doi: 10.1016/j.aej.2020.08.043.

[44] Q. Askari, M. Saeed, and I. Younas, "Heap-based optimizer inspired by corporate rank hierarchy for global optimization," *Expert Syst. Appl.*, vol. 161, Dec. 2020, Art. no. 113702.

[45] D. P. Joshi and K. Sharma, "Effects of grain boundaries on the performance of polycrystalline silicon solar cells," *IJPAP*, vol. 50, no. 9, pp. 661–669, 2012.

[46] J. G. Fossum and F. A. Lindholm, "Theory of grain-boundary and intra-grain recombination currents in polysilicon p-n-junction solar cells," *IEEE Trans. Electron Devices*, vol. 27, no. 4, pp. 692–700, Apr. 1980.

[47] S. Koohi-Kamali, N. A. Rahim, H. Mokhlis, and V. V. Tyagi, "Photovoltaic electricity generator dynamic modeling methods for smart grid applications: A review," *Renew. Sustain. Energy Rev.*, vol. 57, pp. 131–172, May 2016.

[48] L. Wang, Z. Wang, H. Liang, and C. Huang, "Parameter estimation of photovoltaic cell model with Rao-1 algorithm," *Optik*, vol. 210, May 2020, Art. no. 163846.

[49] A. A. Zaky, R. A. E. Sehiemy, Y. I. Rashwan, M. A. Elhossieni, K. Gkini, A. Kladas, and P. Falaras, "Optimal performance emulation of PSCs using the elephant herd algorithm associated with experimental validation," *ECS J. Solid State Sci. Technol.*, vol. 8, no. 12, pp. Q249–Q255, 2019.

[50] A. A. Zaky, M. N. Ibrahim, H. Rezk, E. Christopoulos, R. A. El Sehiemy, E. Hristoforou, A. Kladas, P. Sergeant, and P. Falaras, "Energy efficiency improvement of water pumping system using synchronous reluctance motor fed by perovskite solar cells," *Int. J. Energy Res.*, vol. 44, no. 14, pp. 11629–11642, Nov. 2020, doi: 10.1002/er.5788.

[51] V. Khanna, B. K. Das, D. Bisht, Vandana, and P. K. Singh, "A three diode model for industrial solar cells and estimation of solar cell parameters using PSO algorithm," *Renew. Energy*, vol. 78, pp. 105–113, Jun. 2015.

[52] S. Mirjalili, S. M. Mirjalili, and A. Lewis, "Grey wolf optimizer," *Adv. Eng. Softw.*, vol. 69, pp. 46–61, Mar. 2014.

[53] F. A. Şenel, F. Gökçe, A. S. Yüksel, and T. Yiğit, "A novel hybrid PSO–GWO algorithm for optimization problems," *Eng. Comput.*, vol. 35, no. 4, pp. 1359–1373, Dec. 2018.

[54] C. Kumar, T. D. Raj, M. Premkumar, and T. D. Raj, "A new stochastic slime mould optimization algorithm for the estimation of solar photovoltaic cell parameters," *Optik*, vol. 223, Dec. 2020, Art. no. 165277.

[55] M. Premkumar, T. S. Babu, S. Umashankar, and R. Sowmya, "A new metaphor-less algorithms for the photovoltaic cell parameter estimation," *Optik*, vol. 208, Apr. 2020, Art. no. 164559.

[56] T. Kang, J. Yao, M. Jin, S. Yang, and T. Duong, "A novel improved cuckoo search algorithm for parameter estimation of photovoltaic (PV) models," *Energies*, vol. 11, no. 5, p. 1060, Apr. 2018.

[57] M. H. Sulaiman, Z. Mustaffa, M. M. Saari, and H. Daniyal, "Barnacles mating optimizer: A new bio-inspired algorithm for solving engineering optimization problems," *Eng. Appl. Artif. Intell.*, vol. 87, Jan. 2020, Art. no. 103330.

[58] K. Yu, B. Qu, C. Yue, S. Ge, X. Chen, and J. Liang, "A performance-guided JAYA algorithm for parameters identification of photovoltaic cell and module," *Appl. Energy*, vol. 237, pp. 241–257, Mar. 2019.
[59] X. Chen, B. Xu, C. Mei, Y. Ding, and K. Li, "Teaching–learning–based artificial bee colony for solar photovoltaic parameter estimation," *Appl. Energy*, vol. 212, pp. 1578–1588, Feb. 2018.
[60] Q. Niu, H. Zhang, and K. Li, "An improved TLBO with elite strategy for parameters identification of PEM fuel cell and solar cell models," *Int. J. Hydrogen Energy*, vol. 39, no. 8, pp. 3837–3854, Mar. 2014.
[61] X. Chen, H. Tianfield, W. Du, and G. Liu, "Biogeography-based optimization with covariance matrix based migration," *Appl. Soft Comput.*, vol. 45, pp. 71–85, Aug. 2016.
[62] Z. Chen, L. Wu, P. Lin, Y. Wu, and S. Cheng, "Parameters identification of photovoltaic models using hybrid adaptive nelder-mead simplex algorithm based on eagle strategy," *Appl. Energy*, vol. 182, pp. 47–57, Nov. 2016.
[63] S. Li, W. Gong, X. Yan, C. Hu, D. Bai, L. Wang, and L. Gao, "Parameter extraction of photovoltaic models using an improved teaching-learning-based optimization," *Energy Convers. Manage.*, vol. 186, pp. 293–305, Apr. 2019.
[64] K. Yu, X. Chen, X. Wang, and Z. Wang, "Parameters identification of photovoltaic models using self-adaptive teaching-learning-based optimization," *Energy Convers. Manage.*, vol. 145, pp. 233–246, Aug. 2017.
[65] W. Long, S. Cai, J. Jiao, M. Xu, and T. Wu, "A new hybrid algorithm based on grey wolf optimizer and cuckoo search for parameter extraction of solar photovoltaic models," *Energy Convers. Manage.*, vol. 203, Jan. 2020, Art. no. 112243.
[66] A. M. Beigi and A. Maroosi, "Parameter identification for solar cells and module using a hybrid firefly and pattern search algorithms," *Sol. Energy*, vol. 171, pp. 435–446, Sep. 2018.
[67] G. Kanimozhi and H. Kumar, "Modeling of solar cell under different conditions by ant lion optimizer with LambertW function," *Appl. Soft Comput.*, vol. 71, pp. 141–151, Oct. 2018.
[68] A. F. Nematollahi, A. Rahiminejad, and B. Vahidi, "A novel physical based meta-heuristic optimization method known as lightning attachment procedure optimization," *Appl. Soft Comput.*, vol. 59, pp. 596–621, Oct. 2017.